Accepted Manuscript

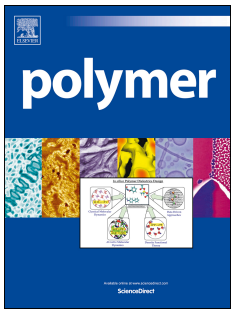

Oxygen diffusivity and permeation through polymers at elevated temperature

Mathew C. Celina, Adam Quintana

PII: S0032-3861(18)30551-2

DOI: 10.1016/j.polymer.2018.06.047

Reference: JPOL 20684

To appear in: *Polymer*

Received Date: 12 April 2018

Revised Date: 6 June 2018

Accepted Date: 16 June 2018

Please cite this article as: Celina MC, Quintana A, Oxygen diffusivity and permeation through polymers at elevated temperature, *Polymer* (2018), doi: 10.1016/j.polymer.2018.06.047.

Oxygen diffusivity and permeation through polymers at elevated temperature

Mathew C. Celina[a], Adam Quintana[b]

[a]*Sandia National Laboratories, Organic Materials Science Dept. 1853, Albuquerque, NM 87185-1411, USA*

[b]*University of New Mexico, Department of Chemical & Biological Engineering, Albuquerque, NM 87131, USA*

Abstract

Oxygen permeability (*P*), diffusivity (*D*) and solubility (*S*) properties are representative of gaseous diffusion in polymers and required for the understanding of polymer physics driven phenomena as well as the quantification of mass transport or polymer degradation processes when diffusion limited oxidation effects result in spatially dependent oxidation behavior. Precise *P, D, S* characterization data for O_2 in polymeric materials at elevated temperatures have not been reported due to instrumental challenges and competitive reactively driven oxygen loss (oxidation reactions), although estimations have been accomplished from indirect measurements of oxidation depths when analyzed with theoretical degradation models. This study offers an overview on experimental approaches which have been applied to the characterization of a range of thin polymer films. As an overview, the O_2 permeation features of three epoxy thermo-set materials, polyimides (Kapton and bismaleimides), and polypropylene for 25 to 140°C were investigated with time-dependent flux measurements and yield permeation data which so far have not been available in the literature. Arrhenius plots of *P* for two epoxies (828/D230 and 828/D400) show the influence of the glass transition temperature, and intriguingly a transition originates mostly through noticeable changes in *S* but not *D*. Multiple material behaviors demonstrating the influence of reactive oxygen loss are discussed. Polymer oxidation chemistry will often interfere with physical permeation measurements at elevated temperatures, in conflict with perhaps the expectation for simple non-reactive O_2 transport. Misleading data may result unless the underlying reactive oxidative loss is considered and compensated for, or permeation data are compared at multiple O_2 partial pressures to validate non-reactive experimental conditions.

Key words: O_2 permeability/diffusivity/solubility, temperature dependence, reactive transport conditions, competitive oxidation, thermo-set polymers and T_g

Corresponding author:
Mathew Celina
Sandia National Laboratories
POBox 5800, MS 1411, Dept. 1853
Albuquerque, NM 87185
Ph: 505-8453551, fax: 505-8449781, Email: mccelin@sandia.gov

1. Introduction

Gas diffusion through polymer materials, usually measured on thin films or membranes, and in particular for water or oxygen is important for many polymer applications [1], including barrier films [2] and encapsulation materials [3]. Of interest are also basic oxygen transmission rates (OTR) through multi-layer sheets [4] or composites materials [5,6]. Gas transport can be characterized with different methods [7] and oxygen permeation is investigated with approaches ranging from commonly used coulometric [1,8] and galvanic [5] to fluorescence quenching sensing [9,10]. Precision gas diffusion studies have been used to characterize some physical ageing processes in polystyrene based polymer films [11] and gas transport can also be approached with molecular dynamics (MD) modeling [12]. Oxygen permeation measurements, in particular when simple OTR are determined, are usually conducted at low temperatures when oxidative reactions for thin films may be negligible but experiments on thicker specimens may be inadvertently biased. Only limited data are available in the literature where O_2 permeation at elevated temperatures has been approached as a systematic combination of physical diffusion and competitive reactive O_2 loss due to oxidation of the film or membrane material itself [13]. For the characterization of polymer aging phenomena it is critically important to distinguish between diffusion physics and reactive loss of O_2 in a material [14].

Polymer material reliability and performance predictions often depend on the quantification of oxidation behavior, both as a function of time and position. A clear understanding of oxygen permeation into any polymer or assembly under investigation is required for modeling of spatially dependent oxidation or predicting the contribution of diffusion limited oxidation (DLO) conditions to accelerated aging studies, whether polymer oxidation is approached via mechanistic-based kinetic models [15-18] or with average oxidation rates utilizing the overall oxygen consumption rate from the auto-oxidation scheme [19-21]. No matter how DLO effects are quantified or predicted, the parameters of oxygen permeability (P_{ox}), as well as diffusivity (D) and solubility (S) are key underlying parameters in the mathematical description of local variations in polymer oxidation [13,14,17,19,21-23].

Oxygen consumption, as part of free-radical oxidation chemistry, is an important complicating factor when O_2 permeation experiments are conducted through thin film polymers in the classic 1D approach. Ideally, the characterization of permeation behavior should be a purely physical process. Unfortunately, material oxidation behavior often interferes with permeation measurements, particularly since the absolute mass transport is often relatively low, and even a limited loss due to oxidative reactions can represent a non-negligible secondary competing process. This is usually more important at elevated temperatures when oxidation rates become a dominant feature, since the activation energies for oxidation rates are often higher than for permeability and hence diffusion limited oxidation becomes proportionally more important when the temperature is raised (i.e. the oxidation rate increases more than the diffusion rate). When DLO applies, corrections for oxidative chemistry have to be made in order to obtain true O_2 permeability measurements. This was demonstrated for elastomers at elevated

temperatures by combining permeative flux measurements with DLO models to correct for the 'reactive' fraction when measuring oxygen permeation [13]. Due to limits in temporal detector response, data acquisition and analysis options (analog signals) at the time, these measurements could not be sufficiently resolved to simultaneously yield P_{ox}, D, and S.

For many materials, basic guidance on permeative properties is available in the literature, mostly as transmission rates at low temperatures [24]. Overview characterization data for transport of small molecules through polymers in terms of P and D are provided in the relevant sections of 'Properties of Polymers' [25] or the 'Polymer Handbook' [26]. The dependence of P, D, S on temperature is given by Arrhenius equations and the activation energy (E_a) for D depends on the 'mean square collision diameter' meaning the E_a for H_2 diffusion is lower than for CO_2, however the interaction of simple gases with the polymer is also weak [25]. For elastomers and glassy polymers the E_a for D is usually no more than 60 kJ/mol with diffusivities at RT in the range of 10^{-9} (PET) to 10^{-5} cm^2/s (silicone), but often the range for which an E_a may apply is not specified [25]. For most elastomers P_{ox} at RT is expected to be between ~ 4 x 10^{-11} and 5 x 10^{-8} ccSTP/cm-s-cmHg, with E_a of similar magnitude as for D; nitrile or butyl rubbers are found at the lower end with natural rubbers or EPDM in the middle and silicone rubbers at the top of the permeability range [13]. For glassy polymers P_{ox} at RT usually falls in the range of 5 x 10^{-12} (PVC) to 3 x 10^{-10} ccSTP/cm-s-cmHg (PS) [25,26]. O_2 permeability of polymers is normally slightly higher than that of N_2. For semicrystalline materials there is much larger variation, and for example N_2 permeabilities between 10^{-13} and 10^{-8} ccSTP/cm-s-cmHg at RT have been reported with fluorinated polymers, polyimides, or polyesters at the lower range [25]. Solubility usually has very low activation energies, therefore the E_a for permeability often matches that of diffusivity [25]. Only limited data exist for O_2 permeability at elevated temperature (see for example our later discussion for polypropylene [27,28]), and competitive oxidation is usually not considered.

In many instances, guidance on basic oxygen diffusion and permeation behavior for epoxies and high temperature composites has been extracted from the examination of DLO profiles, either in discoloration, modulus or perhaps the embrittled degraded layer [15,29,30]. The term total oxidized layer (TOL), being the 1D spatial depth in which all oxidation occurs, was introduced for DLO profiles and was equated with the quantity $\sqrt{D/r}$ assuming either zero or first order dependence of the effective oxidation rate (r) with respect to $[O_2]$ [15,17,31]. This was mostly due to the fact that simple analytical solutions exist for zero or first order, but this approach for TOL is also reasonably appropriate when degradation profiles are relatively steep. However, it also has been shown that bulk oxidative reactions are often better described by a hyperbolic form (i.e. non-specific kinetic behavior) of local oxygen consumption rate versus O_2 pressure (termed a beta-factor (β) dependence in the DLO models introduced by Sandia National Laboratories (SNL) [13,19,21,22] and originally conceptualized by Cunliffe [23]). This affects the spatial profile shape and complicates the estimation of underlying diffusivity, if unknown. As will be shown in a future publication, when oxidation rates and diffusivity are known and modeled profiles are compared with discoloration profiles, for

an epoxy material for example, the approach of using TOL based on color depth for rate over diffusivity estimation can diverge significantly from the actual underlying diffusivity.

At elevated temperatures polymer oxidation chemistry also often interferes with physical permeation measurements, for which misleading diffusivity data may result unless the underlying oxidation rate is considered. Precise P_{ox}, D, S data for many polymeric materials at elevated temperatures do not exist, although estimations have been made from indirect measurements or theoretical approaches (see earlier discussions of TOL). Better known is often the generic oxidation sensitivity of polymeric materials through measurements of their O_2 consumption rates with temperature [32-35], which also led to the conclusion that O_2 permeation at elevated temperature must proceed in competition with oxidation [14,17,19,21,22,36]. For example, epoxies are surprisingly reactive despite their glassy state [37] and polyolefines usually have pronounced induction time behavior with initially low rates that can quickly auto-accelerate [38,39]. Aromatic polymers such as Kapton, BMI (bismaleimides) and similar materials (MVK-14, a high temperature resin system similar to PMR-15) are also known to be sensitive to thermo-oxidation at elevated temperature [30,40-43].

The theoretical description of gas permeation through polymers has employed two distinct models. The first, and most intuitive, utilizes the free-volume theory for diffusivity [44] coupled with a dual-mode sorption (DMS) model for solubility [45]. In this approach, the sorption of a penetrant is considered to occur through either a Henry's Law or a Langmuir sorption isotherm, both of which are considered independent and have distinct diffusivities and solubility coefficients. The free-volume theory grants an analytical description of the diffusivity offering a non-linear Arrhenius plot for polymers above the glass transition temperature (T_g), which resemble experimental data of temperature dependent permeability for rubbery polymers [13]. The introduction of a second mode for penetrant transport offers more material parameters to vary in order to simulate experimental data [45], yet this model fails for certain polymers at high pressures and does not describe the penetrant transport through the polymer phase change at the glass transition.

The second and more contemporary theoretical description of gas permeation comes from the equation of state derived from what is termed the Non Equilibrium Thermodynamics of Glassy Polymers (NET-GP) [46]. Utilizing a lattice fluid domain, the NET-GP equation of state provides sorption isotherms from what is termed the Non Equilibrium Lattice Fluid model (NELF). This model more successfully describes unusual sorption isotherms at high pressures by accounting for polymer swelling and plasticization effects that the DMS model fails to address. Theoretically, NELF may have the capability to describe the unusual temperature variance of solubility through the glass transition temperature as well as anomalous temporal permeate observations, as will be shown in this work, but more detailed quantification of the NELF parameters must be made to verify that this model concurs with the experimental data.

Our current study offers an overview on detailed experimental approaches which can now be applied to characterize thin films of low permeable polymers, for example thermosets below T_g. This can be achieved by ruling out or correcting experimental data for DLO effects and hence significant reactive conditions, and by using computational data analysis to extract diffusivity and solubility from time-dependent measurements. The O_2 permeation features of three epoxy thermo-set materials, Kapton, BMI and polypropylene between 25 and 140°C were investigated and summarized to offer comparative data, which so far have not been available in the literature.

An additional scope of this study is to better understand the influence of T_g resulting perhaps in transitions in the activation energies (E_a) for permeative properties (*P, D, S*), for which there is surprisingly little clarity in the literature. Free volume is often and perhaps simplistically associated with *D*, which, however, may not be a reasonable expectation considering that the chemical interaction features between penetrant and matrix material do not necessarily change at T_g and that *S* should be the more plausible material property being sensitive to material volume changes given by the enlargement of free volume at T_g. A good review on free volume effects and hydrodynamic interactions as the foundation for the development of different models was provided by Masaro et. al. [47]. An excellent overview of gas diffusion through membranes and the dependence on free volume was offered by Sanders and coworkers who emphasized that the Cohen-Turnbull model predicts that diffusion coefficients increase strongly as free volume increases [48]. It may also simply depend on whether the addition of free volume at T_g with increasing temperature results in larger nano-voids heterogeneously distributed in the matrix or addition of extra volume of similar discrete domain sizes as already present below T_g. In the former case we would expect *S* to increase with free volume size since similar diffusion through the matrix material still has to occur, in the latter case we would expect *D* to be affected by overall more free volume of similar size beyond T_g as penetrant transfer should then become more efficient.

2. Experimental procedures

2.1 Materials

Epoxy thermoset materials

Three epoxy thermo-set materials were prepared by blending a diglycidylether bisphenol A resin (Epon 828 obtained from Hexion, CAS# 25068-38-6) with a cycloaliphatic amine (Ancamine 2049 from Air Products Inc., 4,4'-methylenebis(2-methylcyclohexylamine), CAS# 6864-37-5), a polyetheramine (Jeffamine D230 from Huntsman Corp., poly(propylene glycol) bis(2-aminopropyl ether) with approximate M_w 230, CAS# 9046-10-0), and a longer chain polyetheramine (Jeffamine D400 also from Huntsman Corp., CAS# 9046-10-0) in stoichiometric quantities at room temperature (RT). The mixing ratios were 1:0.317 (Epon 828 to Ancamine 2049), 1:0.317 (Epon 828 to Jeffamine D230), and 1:0.61 (Epon 828 to Jeffamine D400), respectively. (Please note that in a related paper describing the oxidation rates of these two epoxies, the stoichiometric ratio of the 828/D230 system should have been 1:0.317 rather than 1:0.61, which was a

typographical error [37]). The Ancamine 2049 system required the addition of 0.25% 1-methyl imidazole as a catalyst to accelerate its cure at RT to more easily obtain a defect free thin film. In this low concentration this catalyst does not affect the material O_2 permeative behavior and cure still proceeds stoichiometrically with the amine. All epoxy systems were initially cured at RT for 24 h and then further post-cured for 1 h at 125°C, except the 828/2049 system was post-cured for 1 h at 150°C; these conditions were sufficient to enable maximum cure conversion. The cure processes also minimized thermo-oxidation during cure while allowing the preparation of thin films on release films placed on a flat laboratory bench top surface via initial cure at RT. The cured 828/2049 system analyzed by DSC has a T_g of 150-155°C, while the 828/D230 system has a T_g of ~ 95°C, and the 828/D400 a T_g of ~ 65°C. Densities are 1.134 g/cc for 828/2049, 1.148 g/cc for 828/D230, and 1.128 g/cc for 828/D400. These densities and also for the materials below were determined based on the Archimedes principle using small samples weighed under air and in isopropanol [49,50].

Kapton

A commercial Kapton polyimide film of 50 µm (2 mils) thickness was used as commercially produced by DuPont. Kapton is mostly amorphous and has a T_g between 360 to 410°C. Its density is 1.41 g/cc. The commercial 50 µm Kapton film is usually Kapton 200 HN which is based on the condensation of pyromellitic dianhydride and 4,4'-oxydiphenylamine, with its partial crystallinity having some influence on permeative properties, even as a function of thickness [51], which hence for Kapton as a generic material type will somewhat vary based on exact constituents, processing conditions and overall crystallinity [52].

BMI and MVK-14

A commercial unfilled composite bismaleimide (BMI) matrix material of 490 µm thickness and a small 505 µm thick sample of cured MVK-14 resins were used as provided by Pochiraju and Tandon who published a nice overview of the high temperature performance of such materials [29]. For BMI a common constituent is 4,4'-bismaleimidodiphenylmethane, but the exact structure of a crosslinked BMI may vary subject to its co-curatives such as 2,2′-diallylbisphenol-A, bisphenol-A bisallyl ether, 4,4′-bis[2-(1-propenyl)phenoxy]benzophenone, or amine based cure mechanisms [53-55]. MVK-14 is a high-temperature unfilled thermosetting polyimide that is recommended as a MDA-free replacement for PMR-15 [43]. Density was 1.3 g/cc for BMI and 1.26 g/cc for the MVK-14.

Polypropylene

A sample of an injection moldable PP grade film was cut from a commercial laboratory PP container and compressed briefly to a thickness of 1.5 mm in a hot press at 180°C. It was allowed to cool slowly under pressure to induce crystallization in a non-quenched manner. Its density was 0.89 g/cc and crystallinity was measured by DSC as ~ 45 % based on a pure crystalline melting enthalpy of 207 J/g [56]. Crystallinity will affect permeability more than diffusivity, since transport occurs predominately in the amorphous fraction which is directly proportional with overall O_2 solubility of the

material [57,58]. Crystallinity may also slightly change during the experiment subject to beginning annealing effects at the highest temperatures.

2.2 O_2 permeation instrumentation

Oxygen permeation experiments were performed on thin film samples using a customized commercial Oxtran 2/21 coulometric permeation instrument (Modern Controls, Inc., Minneapolis, MN, USA). The instrumental setup is based on ASTM D3985-81 [8]. All experiments were conducted with a customized system, where an external permeation chamber holding the sample allows for permeation through a 20x10 mm (2 cm^2) specimen and is positioned in a common temperature–controlled laboratory oven to allow high temperature experiments. The feed gas composition can be adjusted to any O_2/N_2 mixture between 100% N_2 and 100% O_2 partial pressure (p_{O2}), normally at atmospheric ambient pressure equal to 630 Torr in Albuquerque, NM (ABQ). We used standard bottled compressed air, and ultra-high purity O_2 and N_2 as supplied by Matheson. An MKS 247C controller unit with MKS flow controllers (maximum flow 20 cc/min) in combination with multiple switching valves are used to provide different O_2 partial pressures (feed gas composition) and experimental conditions, i.e. to initiate up and down permeation flux experiments (where 'up' means changing the feed gas composition to a higher and 'down' to a lower O_2 concentration). The pick-up gas flow, which collects the O_2 after diffusing through the polymer film, is normally 10 cc/min of pure N_2 with ~ 2% H_2 (provided by Matheson as ultra-high purity N_2 blended with H_2). The measured concentration of O_2 in this detector flow relies on a reaction between O_2 and H_2 utilizing a proprietary catalysis-based sensor and is detected as a signal based on a chemical reaction of oxygen. For some basic total air pressure dependent experiments the feed gas supply was controlled between 630 Torr (ambient pressure in ABQ) and 1350 Torr with a suitable pressure gauge and needle valve.

All permeation measurements were conducted under dry conditions meaning there was no additional swelling subject to moisture retention or perhaps a chance for hydrolytic degradation during high temperature exposure. Dry conditions were assured by the use of dry gases and enough lateral film material mounted in the fixture to prevent inadvertent ambient moisture contamination (O_2 contributions from the film edges were similarly ruled out). Further, all materials were initially conditioned at RT as part of experimental leak checks and the need to remove all dissolved O_2 from ambient storage. Since water diffusion is usually faster than O_2, this also allowed for sufficient time for the samples to dry in parallel with O_2 removal under initial N_2/N_2 conditions.

2.3 Dynamic range and measurement considerations

Our modified external cells offer sample areas between 1 and 10cm^2. Most experiments were run on a 2 cm^2 films for which it is possible to measure permeability (P_{ox}) on the order of 1 x 10^{-14} to 1 x 10^{-7} cc(STP) cm^{-1} s^{-1} $cmHg^{-1}$ (1 x 10^{-12} and 1 x 10^{-5} ccSTP/cm-s-Pa) with suitable variation in film thickness and partial pressure. As shown in this study, when large temperature ranges and different polymers are involved, the permeability (primary transmission rates) will vary greatly. The current system (Mocon 'red' detector) is at the upper experimental limit for a silicone film of 1mm thickness at 80°C (detector overload) and for thick epoxies at RT at the lower limit due to insufficient sensitivity.

For example, a minimum detectable absolute O_2 flux of 0.05 ccSTP/m^2-day (above any baseline) for a 100 µm film of 10 cm^2 size and O_2 feed, yields *P* of 9.2 x 10^{-15} ccSTP/cm-s-cmHg. A maximum flux of 10,000 ccSTP/m^2-day for a highly permeable 1 mm thick silicone film of 1 cm^2 size at 10% O_2 yields a permeability of 1.8 x 10^{-7} ccSTP/cm-s-cmHg. For these two examples the actual oxygen concentration in the detector carrier gas flow of 10 cc/min ranges therefore between 0.0032 and 64 ppm (calculated by converting STP data to RT) which is the useful dynamic range of the detector for this system. In principle, permeation experiments could be conducted on thinner (i.e. 25 µm) and larger films using the commercially provided permeation chamber with a size of 50 cm^2. This would push *P* sensitivity towards a lower 5 x 10^{-16} ccSTP/cm-s-cmHg, however, films with uniform thickness of this size are often not readily available. For practical purposes, we found an external chamber with an area of 2 cm^2 the most useful size for the materials of interest in this study.

Under non-oxidative conditions, usually encountered for low temperature experiments, permeability P_{ox} is easily determined from the instrumentally provided equilibrium flux F_{exp}, thickness *L* and the applied oxygen partial pressure p_{O2} using eq. (1) (note, the receiving side, i.e. detector flow, is always zero in [O_2]).

$$P_{ox} = \frac{F_{exp} L}{p_{O2}} \qquad \text{Eq. (1)}$$

2.4 Determination of diffusivity

For the determination of diffusivity, the set-up is limited by data acquisition and internal detector response behavior. Automatic flux data acquisition is limited by the commercially supplied software to one data point every 2 minutes. Primary flux is visually updated every 6 seconds, which can be manually recorded if necessary, however every 2 minutes there is also a 30 second period during which the signal is not updated. Should manual data recording be required, the experiment is at the limit of a meaningful detector response already. The commercial Mocon system is not designed for fast diffusion measurements at elevated temperature.

Since an external stage is used, there is an additional delay resulting from the time required for the feed-gas composition to reach the polymer film from the valve switch, and for the pick-up gas to deliver the oxygen-enriched flow to the detector. In our experiments the intrinsic delay time between a gas switch (i.e. O_2 switched on) to first detector signal, was measured using a pin hole in a polymer film and found to range between 145 seconds for a 10 cc/min feed and 5cc/min pick-up gas flow (conditions which applied to most experiments reported here) and a delay of 106 seconds when both flows were at 10 cc/min. Based on such delays and intrinsic detector dynamics, i.e. evolution and decay of the experimental signal versus internal detector response delay, any permeation experiments to yield diffusivity should not be shorter than approximately 15 minutes. Permeability can still be measured, but *D* and *S* can no longer be determined from experiments with rapid experimental responses beyond the instrument's capability to successfully acquire time resolved flux data, i.e. when the change in the detector signal is on the order of 2 minutes, which for example occurs when diffusivity is larger than 3 x

10^{-7} cm^2/s for a 100 µm film. For those reasons, some diffusivity values for higher temperatures could not be determined, despite the availability of permeability in equilibrium. There are no constraints for permeation equilibrium experiments which may take a few days, e.g. 72 h for a 100 µm film could yield a diffusivity of 1.4 x 10^{-10} cm^2/s (95% to signal equilibrium time).

2.5 Film thickness considerations

Thickness selection is a compromise between the need to minimize oxidation reactions and a suitable level of O_2 mass transport (flux) to be in line with detector sensitivities. Particularly at elevated temperatures, there are limits in experimental feasibility because oxidation reactions generally have activation energies higher than that of permeation (on the order of 70-140 kJ/mol versus 10-40 kJ/mol usually observed for permeation). This means chemically driven O_2 loss will dominate oxygen transport at high temperatures. Films should be thin to minimize oxidative loss, yet thicker films may be required to reduce the actual flux as to not overload the detector. For the experiments reported here, mostly thin films of ~ 100 to 200 µm were used to minimize interference from oxidation. At high temperatures, generally above 100°C, the resulting flux was significant, but not yet outside the linear detector response. Upper experimental temperature limits for diffusivity were dependent on the time response of the experiments, dictated by the intrinsic speed of the detector and data acquisition limits. Flux can be reduced and the experiment extended (for diffusivity) by using thicker films, but oxidative loss can then be a major complication (e.g. oxidation rates for epoxies can be significant [37]), particularly at elevated temperature.

In many instances for the characterization of O_2 transfer through polymers, flux measurements may be used to establish basic transmission rates for specific thickness [24]. However, such measurements may not yield the true material permeability constant unless oxidative loss can be ruled out (applicable mostly to low temperature data) or is taken into account via a correction factor using diffusion limited oxidation models [13]. Complications through oxidative chemistry during the experiment can be excluded as long as different O_2 partial pressures yield the same permeability constant. In this study, nearly all data were obtained at minimum from a comparison of 100% and 21% (air) up and down (switching O_2/air on and off) experiments.

2.6 Oxidation during permeation

We note that nearly all studies dealing with the measurement of oxygen permeation to determine permeability do not address the competitive nature of oxygen loss due to oxidation of the material test specimen [1,2,5,6], which due to the nature of these processes will be highly thickness dependent. At high temperatures or for thicker material test specimens when oxygen loss due to chemical reaction is significant, the experimental determination of O_2 permeability becomes more challenging. The measured fluxes must then be corrected for a chemically driven loss component [13]. The situation is further complicated by other factors, i.e. a) there are indications that for high fluxes the sensor readings may lose linearity in the upper regime (e.g. actual signal counts above 10^6 for the detector used herein), b) ongoing oxidation of the film will lower the permeability over time [22], and c) because of oxygen consumption it may take

longer for equilibrium conditions to be established depending on transport regimes. For those reasons permeability was measured on a small film of 2 cm^2 (good sensor range) and pure oxygen readings were taken quickly followed by repetitive reduction in oxygen partial pressure yielding additional readings. If necessary, these primary measurements were then corrected for oxidative loss using the basic auto-oxidation DLO model to yield the underlying permeability constant [20]. Model corrections require knowledge of a beta factor [19,21], which here was on the order of 1 to 10, obtained both by separate 'beta experiments' for oxidation rate dependency on O_2 partial pressure, and collective correction of multiple measured fluxes with a best fit for a single beta factor through residual error minimization. These aspects will be discussed further in a separate publication. Considering our instrumental ability and understanding of these materials, the permeability data provided here are representative for the higher temperatures investigated.

2.7 'Reactive diffusion model' (Fickian diffusion with reactive term for oxidative conditions)

As discussed above, when oxidation chemistry competes with physical O_2 transport, permeability and diffusivity can only be determined when a reactive term is applied to the established gas-solid transport relationships. For the determination of P_{ox}, D, and S data, Fick's second law (e.g. the mass conservation equation) requires an added oxygen loss term to accommodate free radical oxidation of the solid polymer and can be solved numerically, as shown below:

The rate equation (eq. (1)) describing oxidation has been established from the basic auto-oxidation scheme (BAS) and is an explicit function of dissolved oxygen concentration, where k_1 and k_2 are overall rate constants resulting from the BAS mechanism assuming either uni- or bi-molecular radical termination. Both allow for identical oxygen concentration dependence [19,21], long kinetic chain lengths, and that hydroperoxide branching (closed loop model allowing for auto-acceleration of oxidation rate [18,38]) is unimportant in the time frames of interest.

$$-\frac{d[O_2]}{dt} = \frac{k_1[O_2]}{k_2[O_2]+1} = \phi \qquad \text{Eq. (1)}$$

The resulting partial differential equation when combining the rate equation with Fick's 2nd law of diffusion then describes the overall mass balance of dissolved oxygen as given in (eq. (2). Since oxidation rate (ϕ) is commonly given in units of mol/g-s the material density is required to find standard concentration units, then in mol/cc-s.

$$\frac{\partial[O_2]}{\partial t} = \nabla \cdot (D\nabla[O_2]) - \frac{k_1[O_2]}{k_2[O_2]+1} \qquad \text{Eq. (2)}$$

The diffusion coefficient is related to oxygen permeability ·($P_{ox} = DS$), and S is the solubility of oxygen defined by Henry's Law [19,22]. By multiplying the resulting

equation by a factor $\left(\frac{L^2}{p_0 P}\right)$,$\left(\frac{L^2}{p_0 P_{O2}}\right)$, where L is a reference thickness, p_0 is the external oxygen partial pressure, and defining the dissolved oxygen concentration as the product of solubility and oxygen partial pressure (Henry's law), the resulting DLO equation becomes a unit-less function eq. (3)) of relative oxygen partial pressure $\left(\theta = {p_{O_2}}/{p_0}\right)$, assuming that solubility and diffusivity are homogeneous [19,22]. This assumption is expected to break down at high pressures, where the thermodynamic consideration of a rubbery or glassy polymer combined with plasticization and swelling effects predicts a concentration dependence of both solubility and diffusivity of gas penetrants [46]. However, for pressures of common interest (i.e. for oxygen partial pressures below 1 atm), these effects are expected to be only nominally present. Therefore, the analysis presented hereafter is valid for the limit of low pressures where permeability is independent on pressure and Henry's law is valid.

Considering the one-dimensional gas transport through the thickness (smallest dimension) of the thin film results in the normalized equation for Fick's second law as given below (eq. 3). The spatial and time dimensions are normalized with respect to L and L^2/D respectively and are specified by the Greek letters χ and τ.

$$\frac{\partial\theta}{\partial\tau} = \frac{d^2\theta}{d\chi^2} - \frac{\alpha\theta}{\beta\theta+1} \qquad \text{Eq. (3)}$$

For a simulation of the thin film permeation experiments, the boundary condition at the exposed side is at full partial pressure ($\theta(0,\tau) = 1$) and the measured side is at zero partial pressure ($\theta(1,\tau) = 0$). The parameters α and β are the normalized rate constants defined as $\frac{k_1 L^2}{D}$ and $k_2 S p_0$ respectively and are related to the O_2 pressure dependent oxidation rate given in eq. (4) [19,21,23]:

$$\frac{\alpha}{\beta+1} = \frac{\phi_0 L^2}{P_{ox} p_0} \qquad \text{Eq. (4)}$$

Here it is pertinent to address the normalization of the model parameters. The dependent variable θ, and main output of the model equation (eq. 3), is the temporal spatially variant partial pressure of oxygen normalized by a specific partial pressure (p_0). For an experiment measuring the oxygen flux from ambient air to pure nitrogen, the normalizing pressure will be the partial pressure of oxygen at ambient air conditions to confer with the relevant boundary conditions (e.g. $\theta(0) = 1$). This specification implies that the value β is also specified at this pressure, recalling the definition $\beta \equiv k_2 S p_0$ [13]. For an experiment probing the oxygen flux under pure oxygen, the normalizing partial pressure will be different from the ambient case to likewise confer with the boundary conditions.

To maintain consistency, the value of β under pure oxygen must also be specified with this pressure rather than the value used under ambient conditions. Therefore, it is convenient to specify β at one pressure (e.g. ambient air throughout this study) and then multiply by the pertinent ratio of pressures to generate the correct value that is consistent with the normalization and boundary condition requirements [13].

The solution to equation (3) is available numerically through any algorithm that can solve a non-linear parabolic partial differential equation (PDE). One drawback of using a PDE solver typically found in computational analysis packages is the time required to reach a solution, as the efficiency of the fitting method, which usually requires numerous sequential solutions, is limited by the efficiency of the PDE solution method. For example, a typical time cost to compute a solution and perform post processing necessary for our specific application of a non-linear time dependent parabolic partial differential equation using a PDE solution package typically found in scientific computational packages is on the order of seconds. Although this time is reasonable for a single solution, we will need to vary the model parameters to converge with our minimization requirements requiring up to thousands of solutions leading to a total computation time on the order of hours. To overcome such limitations the method used in this study (eq. (5)) utilizes an adaptation of the Crank – Nicholson implicit method [59] (k is the time index, i the spatial index and $\boldsymbol{\theta}_k$ is the normalized pressure spatial vector at time point k), with the matrix and reaction definitions shown in eq. (6) and (7) respectively.

$$(a+2)\boldsymbol{\theta}_{k+1} = \mathbb{A}\boldsymbol{\theta}_k - R(\boldsymbol{\theta}_k) \qquad \text{Eq. (5)}$$

$$\mathbb{A} \equiv \begin{bmatrix} a_1 & \cdots & & \cdots & 0 \\ 1 & a & 1 & \cdots & 0 \\ 0 & \ddots & \ddots & \ddots & 0 \\ 0 & \cdots & 1 & a & 1 \\ 0 & \cdots & & \cdots & a_N \end{bmatrix}$$

$$a = \frac{(\delta\chi)^2}{\delta\tau} - 2$$

$$a_1 = \frac{(\delta\chi)^2}{\delta\tau} + \frac{\alpha(\delta\chi)^2}{\beta+1} \qquad \text{Eq. (6)}$$

$$a_N = 1$$

$$R\left(\theta_{i,k}\right) = \frac{\alpha\theta_{i,k}(\delta\chi)^2}{\beta\theta_{i,k}+1} \qquad \text{For: } i = 1,2 \ldots N;\ k = 0,1, \ldots \infty \qquad \text{Eq. (7)}$$

The matrix $\mathbb{A}$ is of size $N \times N$ and is derived from the N equations of each spatial index of the equidistant position points, derived from a Taylor Series approximation of eq. (3). The quantities $\delta\chi$ and $\delta\tau$ are the spatial and time steps respectively and are specified by using a value of a that gives convergent and efficient solutions. A value for a of zero, as used in this study, is suitable for moderately oxidative profiles, and the lower limit of -2 implies an infinite time step considering the normalization condition $L = (N-1)\delta x$. For more severe oxidative conditions, a larger value of a will grant a more accurate solution with the tradeoff of requiring more time steps as well as more computational time and computer memory to reach equilibrium. The values a_1 and a_N as well as the first and last rows of $\mathbb{A}$ are specified by imposing the specific boundary conditions mentioned above. The initial pressure vector $\boldsymbol{\theta}_0$ determines the starting profile of the solution and must be determined by either the solution of the steady-state DLO equation (eq. 3) at that initial pressure or from some known time of a non-equilibrium solution. The boundary point $\theta_{1,k}$ is either 1 or 0 depending on which direction the O_2 partial pressure condition is applied (i.e. a specific p_0 or 100% N_2, respectively), and the opposite boundary point is zero. Normalizing the pressure profile by the inlet pressure, while imposing an initial profile with the same normalizing pressure, allows us to model the change between O_2 partial pressures from any initial pressure.

This recursive matrix equation is easily implemented in any computational programming language and has the ability to provide a quick solution depending on the choice of N and computer hardware. The method's ability to maintain a stable convergent solution relies on the choice of $\delta\chi$ and $\delta\tau$, which can be regarded as just one open parameter if the value of a (eq. 6) is restricted to a specific value. The solution vector is recursively averaged between time points to decrease the absolute error (essentially turning a forward difference into a central difference in time) of the calculation and to give a continuous spatial partial derivative at the exit boundary.

The exit flux (eq. 8) as a function of time is calculated using a forward difference at the exit side which is then multiplied with constants associated with Fick's first law. The Euclidian norm of the difference from the experiment with the interpolated solution is used as the minimization error to fit for the correct P_{ox} and D values. These values are found by a branched fitting approach, which finds the best fitting D at every P_{ox} trial. A second source of error incurred from the non – instantaneous pressure switching was found to induce a time offset between 1 and 3 minutes based on separate experiments probing this offset. However, it is advantageous to allow this offset to be an open variable in the minimization, because D is sensitive to the time to rise. Thus, the time offset is used as an auxiliary variable, linked to experimental realism, to minimize the error before P_{ox}, D minimizations.

$$F_{L,k} = -D\frac{\partial C}{\partial x}(t_k, L) = -\frac{P_{ox}p_0}{L}\frac{\partial \theta}{\partial \chi}(\tau_k, 1) = \frac{P_{ox}p_0\theta_{N-1,k}}{L(\delta\chi)} \quad \text{Eq. (8)}$$

In situations when the competing effects of polymer oxidation are negligible (i.e. for thin films or materials at low temperatures) the consumption term in equation 3 may be set to zero which also grants a non-trivial analytical solution to the underlying PDE. The analytical expression for the normalized exit gradient when initially desorbed and instantaneously exposed at the entrance surface is expressed in eq. (9). The recursive matrix solution (Eq. 5) of identical conditions was compared to the analytical solution and was found to have a maximum deviation of less than 0.2%.

$$\frac{\partial \theta}{\partial \chi}(\tau, 1) = 1 + 2\sum_{n=1}^{\infty}(-1)^n \exp(-n^2\pi^2\tau) \quad \text{Eq. (9)}$$

When oxidation is estimated not to be a concern, the established time-lag method Eq. (10), which is derived from the temporal integral of Eq. (9) leading to the time dependent molar accumulation of oxygen (Q), can also be used for diffusivity extraction. However, this method requires integrating the experimental flux, which will incur an error dependent on the method of numerical integration and resolution (smoothness of flux points). Another drawback is the inability to deduce a time offset induced from the non-instantaneous pressure switch. With the ability to fit the experimental output directly and to account for oxidative loss and time offset, the recursive matrix solution fit is superior to the time-lag method in these experiments.

$$lim_{t\to\infty} Q(t) = \frac{DC_1}{L}\left(t - \frac{L^2}{6D}\right) \Rightarrow D = \frac{L^2}{6t_0} \quad \text{Eq. (10)}$$

$$f_c \equiv \frac{F_{exp}}{F_{ideal}} = -\frac{\partial \theta}{\partial \chi}(\tau \to \infty, 1) \quad \text{Eq. (11)}$$

The model of a time dependent exit flux, as described in Eq. (8), also grants the quantification of the equilibrium flux reduction due to oxidation, which is defined as the ratio of experimentally determined equilibrium flux (F_{exp}) over the equivalent flux with no oxidation (ideal). The change from the ideal flux to the experimental flux under oxidative conditions, and the corrections that need to be applied, was first addressed for high temperature elastomer permeability characterization using an iterative calculation [13]. The current model and its numerical solution approach allows us to more easily define and calculate a 'flux correction factor' (Eq. (11)) as long as ϕ, L, p_{O2}, an estimation of β, and experimental fluxes are available (discussed later in section 3.2), as well as the oxidative loss fraction, given by 1-f_c. The flux correction factor (f_c) represents the ratio of

actual flux (F_{exp}) over ideal O_2 flux (F_{ideal}). This model can also be used to guide estimations and establish the experimental boundaries for high temperature permeation experiments by extrapolation of permeability obtained under low temperature non-oxidative conditions.

3. Results and discussion

3.1. Polyimides (Kapton and BMI)

Initial experiments focused on a commercial Kapton film (50 µm). This was done to evaluate the size and operation of the external permeation cell, thermal control conditions and evaluate the instrument in terms of time response and dynamic detector sensitivity. We also developed the appropriate mathematical framework to extract *D* and *S* from the time-dependent flux measurements. Fig. 1 shows examples of the flux responses and Fickian diffusion fits for air and pure O_2 measurements at 65°C. Switching the feed gas supply from N_2 to air/O_2 and then back to N_2 yields nearly identical data for P_{ox}, *D*, and *S*. Note that in the latter case, the computational boundary and initial conditions will be different from the former (e.g. $\theta(0) = \theta(1) = 0$) since both surfaces are exposed to zero O_2 under desorption and the film already contains dissolved O_2 in equilibrium (different initial pressure loading). Fig. 2 shows the corresponding temperature series for oxygen and air data, for which the flux response at 80°C is then quite fast and therefore represents an upper limit for the meaningful determination of *D* and *S*. However, additional P_{ox} data are available at higher temperatures from fast equilibrium flux measurements at a range of partial pressures chosen to stay within a reasonable detector response level. It was possible to obtain equilibrium P_{ox} data for air, 50/50 O_2/air and 100% O_2 up to 150°C. The beginning of DLO conditions was observed beyond 150°C, i.e. a reduced flux at the lower O_2 partial pressures was strongly noticeable even for the thin film of 50 µm (see additional discussion of those trends in 3.5.4). The Arrhenius plot for P_{ox} is included in Fig. 3 and shows linear behavior with an activation energy (E_a) of 22 kJ/mol. The corresponding *D* and *S* data when available (see Table 1 later) are included in Fig. 4 and Fig. 5, respectively. As an example, a 65°C air experiment for Kapton yields D = 7.23 x 10^{-9} cm^2/s, in comparison with D = 7.73 x 10^{-9} cm^2/s when analyzed with the traditional time-lag method (Fig. 6) [1,60,61]. Figs. 3,4,5 also includes all data from the characterization experiments of the other polymers in this study.

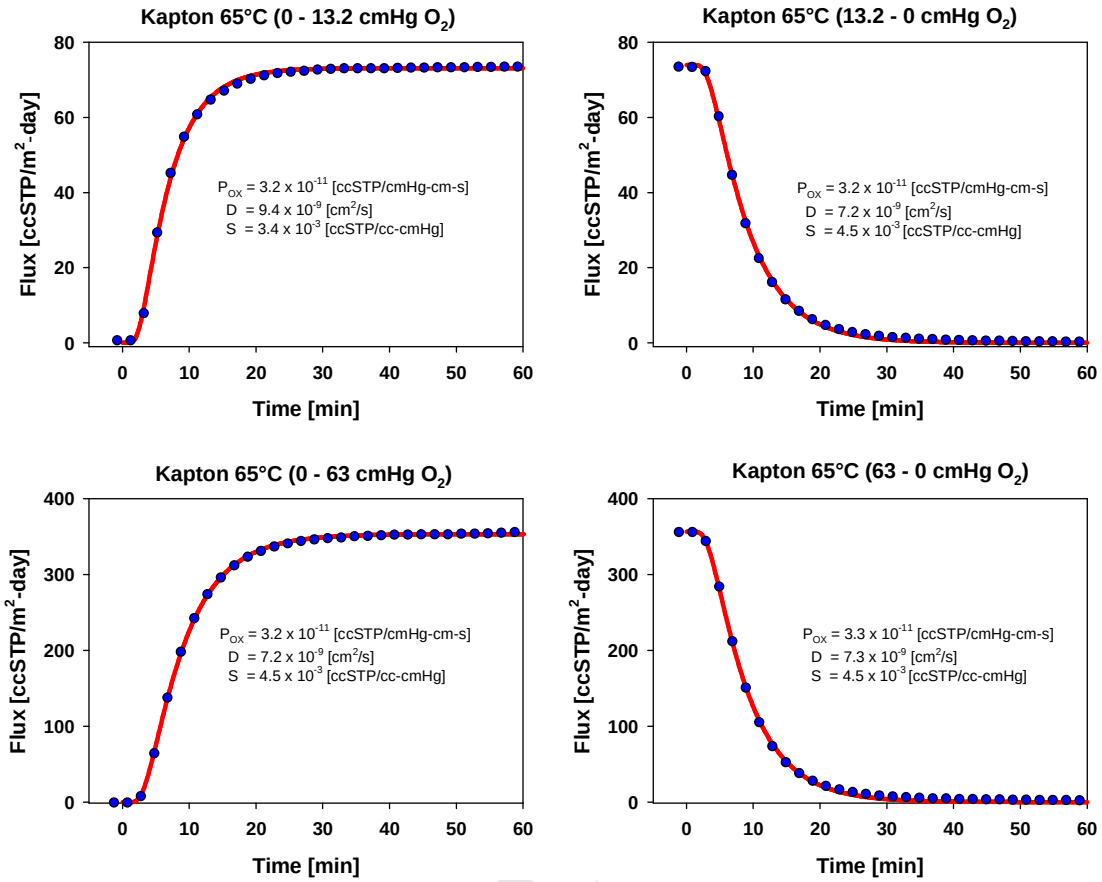

Fig. 1 Flux measurements under air and O_2 conditions for a 50 µm thick Kapton film. These yield *P*, *D*, *S* data when fitted with a Fickian diffusion model (solid line through the experimental data).

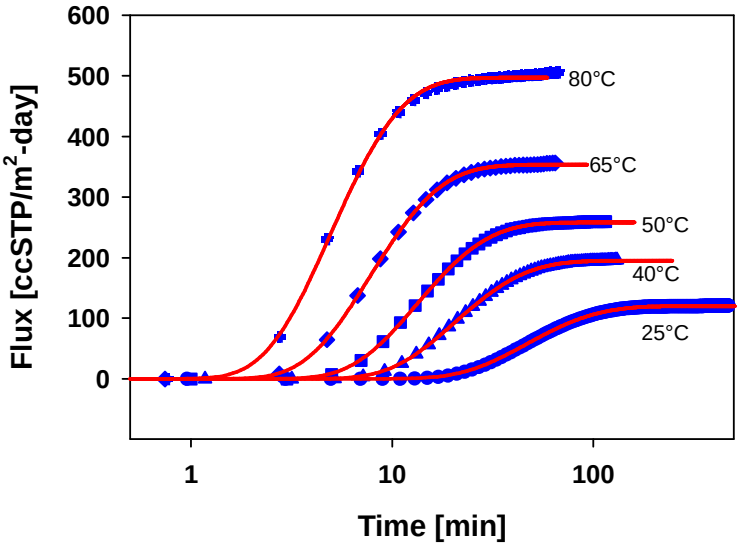

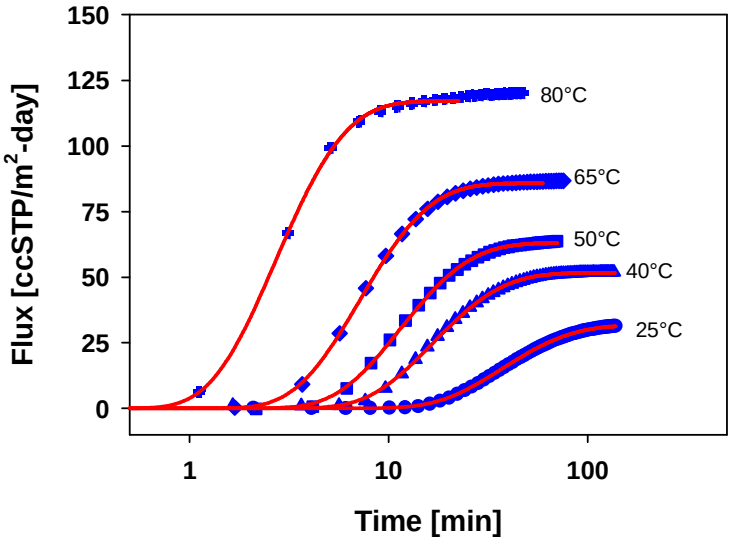

Fig.2 Flux measurements with temperature for a 50 µm Kapton film for pure O_2 (0 to 63 cmHg, upper figure) and under air (0 to 13.2 cmHg, lower figure), both fitted with a Fickian diffusion model (solid line through the experimental data).

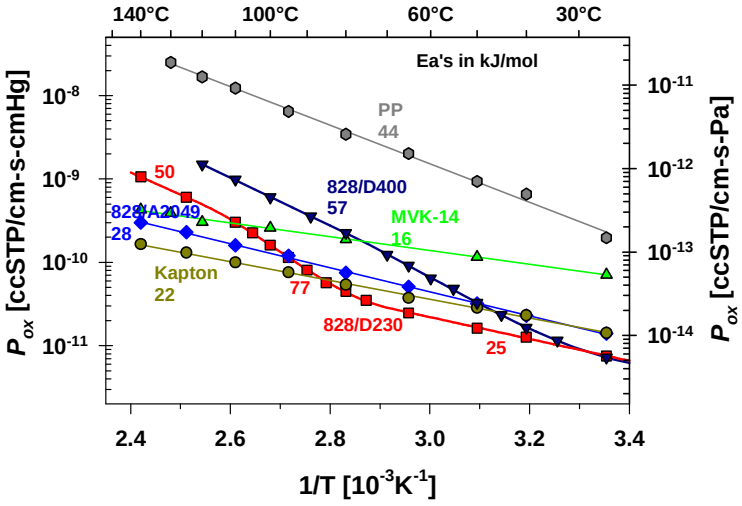

Fig. 3 Arrhenius plot for permeability (P_{ox}) of Kapton, MVK-14, Epoxies 828/A2049, 828/D230, 828/D400 and PP. E_a's range from 16 to 77 kJ/mol as indicated on slopes.

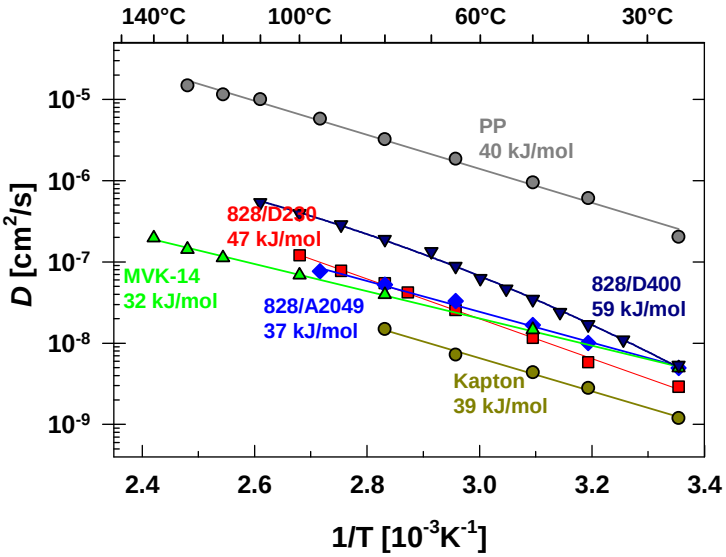

Fig. 4 Arrhenius plot for diffusivity (*D)* of Kapton, MVK-14, Epoxies 828/A2049, 828/D230, 828/D400 and PP.

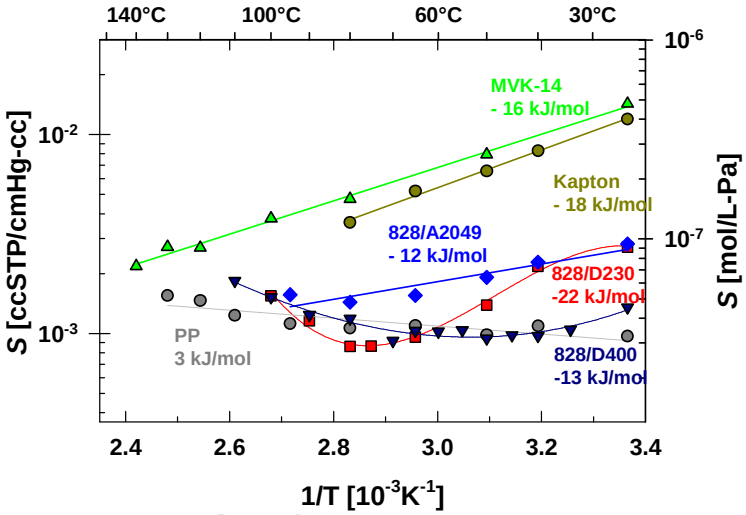

Fig. 5 Arrhenius plot for solubility (*S)* of Kapton, MVK-14, Epoxies 828/A2049, 828/D230, 828/D400 and PP.

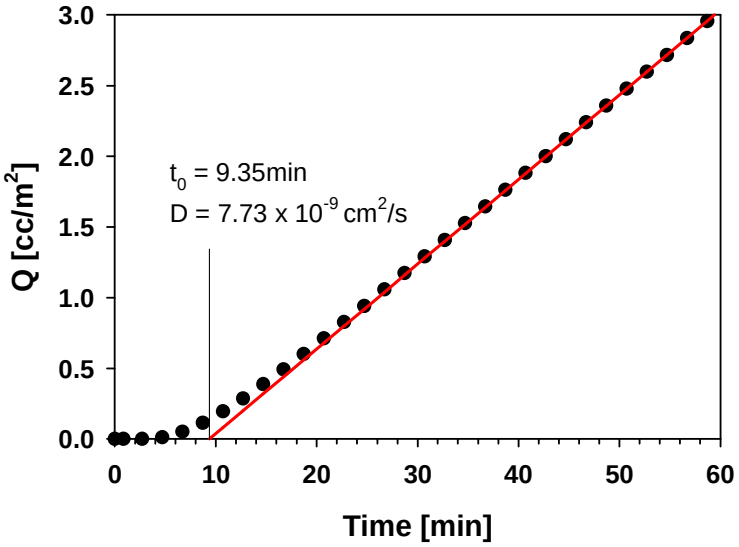

Fig. 6 Traditional time-lag method for determination of *D* from the integrated flux for Kapton at 65°C (air).

Another polyimide, kindly provided by G. Tandon [29], was available as a generic BMI composite matrix material, but with a rather significant thickness of 490 µm. Knowing that Kapton has the beginning of DLO effects at 150°C for a thickness of 50 µm, it was questionable whether P_{ox} for a thicker material could be easily measured at elevated temperatures. This assumes that a BMI material has similar permeability features as a Kapton polyimide (a reasonable assumption as a guiding approach). A screening study showed that O_2 transfer could not be detected for this material over 30 mins at 200°C, 3 hours at 160°C or 70 hours at 120°C. For Kapton, the flux is in equilibrium (99%) at 120°C after 4.7 minutes, hence for ten times the thickness and similar diffusivity, the permeation experiment for BMI at 120°C should have been completed within 470 minutes (~8 h). Similarly, at 80°C the O_2 flux of 575 cc/m^2/day for 51 µm Kapton film is at 99% equilibrium after 16 mins, and a 490 µm material of identical permeability will have a flux of ~ 60 cc/m^2/day after ~ 24 hours. The lack of any measurable O_2 flux over 300 h at 80°C may suggest a BMI material with very low permeability on the order of 1 x 10^{-12} ccSTP/ cm-s-cmHg. However, this is unlikely considering that the lowest epoxy and Kapton data show P_{ox} on the order of at least 5 x 10^{-11} ccSTP/ cm-s-cmHg and D = 2 x 10^{-8} cm^2/s for this temperature. A more likely scenario is still complete DLO control for 490 µm BMI at 80°C due to significant oxidation rates.

The potential complication due to DLO is demonstrated by its influence on modeled permeation experiments at 80°C. An extended 500 h experiment at RT for this BMI yielded P_{ox} = 8 x 10^{-12} ccSTP/cm-s-cmHg and D = 1.2 x 10^{-9} cm^2/s from an equilibrium flux of only ~ 9 ccSTP/m^2/day. P_{ox} and D for 80°C were then estimated with average E_a's (19 kJ/mol for P_{ox} and 35.5 kJ/mol for D) obtained from Kapton and MVK-14 (discussed later), hence assuming similarity with other polyimides. Fig. 7 shows the predicted flux responses for a 500 µm material with assumed P_{ox} = 2.6 x 10^{-11} ccSTP/cm-s-cmHg and D = 1.1 x 10^{-8} cm^2/s at 80°C as a function of varying oxidation rates under pure O_2. At the highest oxidation rate the permeative behavior is completely controlled

by DLO. An expected flux of ~ 28 cc/m^2/day will drop to a just noticeable 2 cc/m^2/day for ~ 1 x 10^{-10} mol/g/s, and zero flux if an oxidation rate of 1 x 10^{-9} mol/g/s is applied in model predictions. Oxidation rates on the order of 1 x 10^{-10} mol/g/s at 80°C have been observed for a number of epoxies, some are summarized in [37], which are then also considerably DLO controlled in the 0.5 mm thickness range (see Figs. 8 a and b later). It is reasonable to propose that this BMI material must have higher oxidation sensitivity than 1 x 10^{-10} mol/g/s at 80°C, which explains the difficulties of measuring P_{ox} for the sample thickness of 490 µm at this temperature.

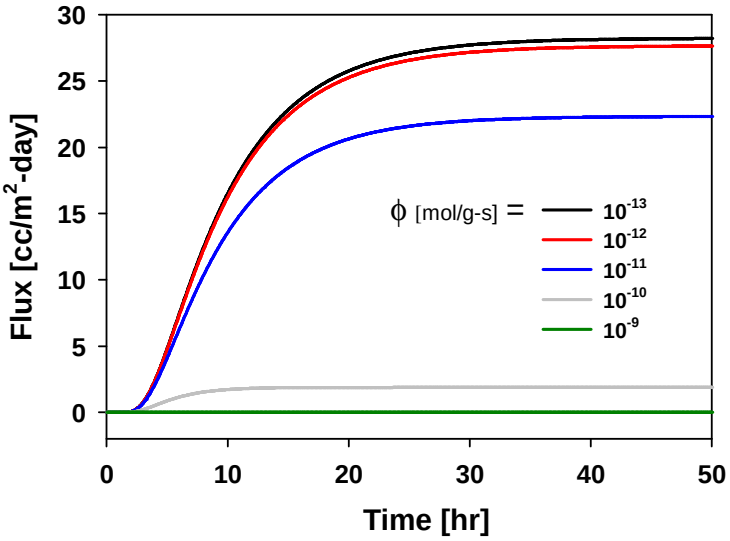

Fig. 7 Reduction in flux with increasing oxidation rate for pure O_2 conditions for a simulated 500 µm thick BMI material at 80 °C. Parameters are P_{ox} = 2.6 x 10^{-11} ccSTP/cm-s-cmHg, D = 1.1 x 10^{-8} cm^2/s, ρ=1.3 g/cc, p_{O2}=63 cmHg, ß=1.

3.2. Epoxy materials

Two epoxy systems were studied that previously had been examined for their oxidation sensitivity and showed very linear Arrhenius behavior for oxidation rates [37]. As shown in Fig. 3, the temperature dependence of P_{ox} for the 828/D230 system shows a strong influence of T_g at ~ 95°C, whereas the 828/A2049 system displays perfect linear Arrhenius behavior. The T_g for this material (~ 155°C) is above the highest temperature examined. Interestingly, below T_g the activation energies for P_{ox} are very similar with 22 kJ/mol for Kapton, 25 kJ/mol for the 828/D230 and 28 kJ/mol for the 828/A2049 epoxy. For the 828/D230 system the E_a increases to 75 kJ/mol during the T_g transition and then approaches a value of 55 kJ/mol above T_g. All individually determined data for P_{ox}, D, S have been included in summary plots (see Fig. 3 to 5) and Table 1.

For both epoxies, P_{ox} for the higher temperatures was determined using the mathematical model discussed in section 2.7. This means that any partial pressure (p_{O2}) dependent permeability was corrected with available oxidation rates [37]. Much of the data are averages of O_2 and air experiments, with D also determined from sorption and desorption experiments. The effects of oxidation on the characterization of these two materials are documented by the predicted flux correction factors with temperature. Figs. 8a and b

(828/A2049 and 828/D230, respectively) show the flux correction factor for pure O_2 and air conditions with varying thickness. For these calculations β was estimated at 5, with the density measured as ~ 1.16 g/cc. It is clear that without taking oxidation into account any experimental permeability above ~ 80°C will have large uncertainty. Unless oxidation is severe, and the flux correction factor drops below 0.2, oxidation effects can be accommodated with the 'reactive diffusion model' to enable high temperature P_{ox} measurements for polymers. Such numbers, as provided in Table 1 are not available in the existing literature.

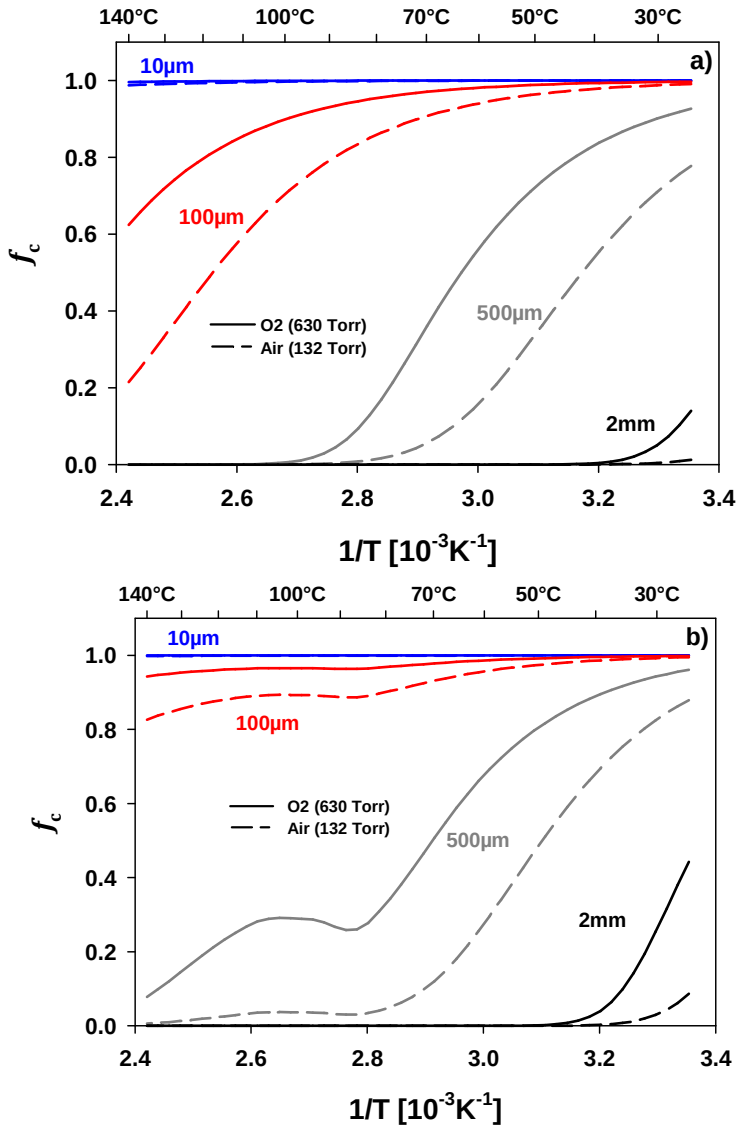

Fig. 8 Flux correction factors for epoxies as a function of temperature and film thickness. Curves were generated with interpolated permeability (see Fig.3) and oxidation rate values [37], and using β= 5 (normalized with ambient partial pressure). Permeative fluxes at elevated temperature are reduced due to significant material oxidation, even for a 100 µm film. a) Epon828/A2049; b) Epon828/D230 with the irregular behavior at ~ 90 °C due to T_g with changes in S.

When the diffusivity and solubility are determined for the 828/D230 system it is surprising to observe that the T_g influence on P_{ox} originates from changes in solubility (Fig. 5) rather than diffusivity (Fig. 4), where the latter displays reasonably linear Arrhenius behavior. It is unclear based on the existing literature why solubility is the driver for T_g effects on P_{ox}, but diffusivity does not show a behavior related to increased mobility at T_g as would be expected. For instance, an increase in the activation energy of diffusivity has been observed for polyvinyl acetate after heating above T_g and a thermodynamic argument was made that this was primarily due to the influence of van der Waals forces between ordered sections of the quasi-crystalline liquid polymer [62]. This suggests that a purely amorphous polymer would not experience any change in activation energy for diffusivity through T_g, as would be appropriate for these epoxies.

An epoxy system of Epon 828 cured with Jeffamine D400 was added to this study to explore if its lower T_g (~ 65°C) would have a similarly pronounced effect on its permeation behavior. There are indications of a weak transition in the Arrhenius plot of P for this material at lower temperatures between 25 and 40°C (Fig. 3), which can be emphasized in the plot of E_a as shown later (see conclusion). The low temperature E_a for 828/D400 between RT and 40°C is 42 kJ/mol. Oxidation at high temperatures is not an issue for this material, consistent with the primary measured P_{ox} not being dependent on p_{O2} up to 130°C, since P_{ox} is much higher for this epoxy system than for the 828/D230 or 828/A2049 materials. This also implies that the relevant oxidation rates for 828/D400 cannot be much higher than for 828/D230. It appears that the higher concentration of polyether segments is beneficial to enhanced permeability (Fig. 3) originating from diffusivity (Fig. 4) above temperatures of 40-50°C, but does not increase the oxidation sensitivity significantly.

3.3. High temperature thermoset MVK-14

MVK-14 is a thermoset material where the high temperature performance has been of interest. It is well-known that diffusion limited oxidation behavior occurs at high temperatures and its O_2 diffusion properties have been estimated from the depth of the Total Oxidized Layer (TOL) [15,17,31,36,63]. However, the underlying oxidation rates, as well as pressure dependence of rate on partial pressure (applicable kinetic model), and solubility at high temperature, which all need to be considered for better interpretation of TOL data, are often unknown. Hence, TOL assessments to yield P_{ox}, D, S, estimations have some degree of uncertainty and at best offer an order of magnitude approach.

An MVK-14 sample was therefore included in our overview study, also since it represents a thicker (505 µm) material where oxidation is expected to interfere at high temperatures. Because of the thickness, the evolution of the flux response is slow as shown in Fig. 9 (compare with the Kapton data in Fig. 1 and 2), but nevertheless the material still shows strong equilibrium fluxes. This is consistent with P_{ox} being considerably larger for the MVK-14. Reasonably linear Arrhenius behavior was observed for all three properties, with E_a's of 11 kJ/mol for P_{ox}, 30 k/J/mol for D and -18 kJ/mol for S (see Figs. 3 to 5). The flux and P_{ox} could be determined up to 140°C without corrections for oxidation (no partial pressure dependence in permeability), which implies

that this material must have the lowest oxidation rates of the Kapton, BMI and epoxy materials compared in this study.

However, for the 130 and 160°C flux data ongoing creep behavior is observed (as discussed later) and the 160°C is clearly affected by oxidation as the flux is significantly reduced. A thinner material here, ideally 50 to 100 µm, would reduce the oxidative component, but primary detector response for oxygen would be at the upper feasible range, all an issue of dynamic experimental sensitivity based on equilibrium flux F_{exp} as a function of P_{ox}, p_{O2}, L (eq. (1)) and oxidation rate ϕ.

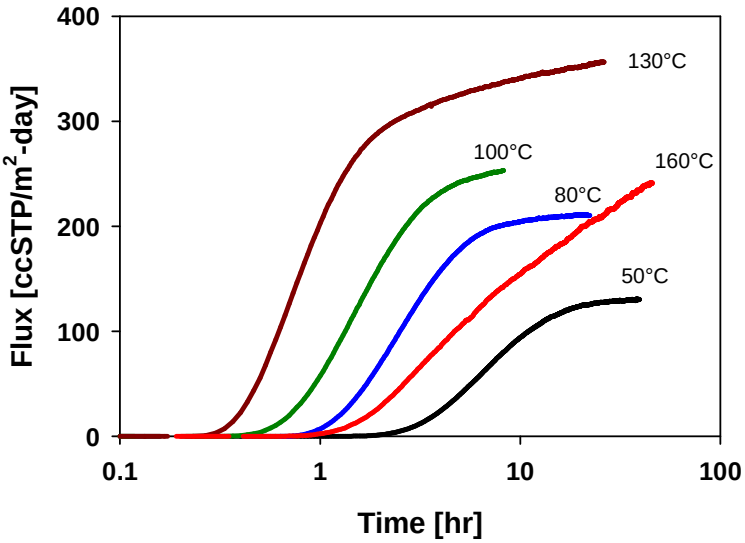

Fig. 9 Reduction of flux due to oxidation for a 505 µm MVK-14 material for pure O_2 (630 Torr). The flux at 160°C is lower than at 130°C and equilibrium times are extended.

3.4. Polypropylene

For a range of elastomers, such as nitrile, neoprene, butyl, EPDM or PU materials permeability has shown curvature in Arrhenius plots [13]. In comparison with the rather linear behavior for two epoxies, the Kapton and MVK-14, it was therefore of interest to also examine a semi-crystalline material such as polypropylene. Since stabilized PP has a very low oxidation rate and also a relatively high permeability, competitive oxidation is not an issue, even for a 1.5 mm thick sample; measurements are easily taken at different partial pressures over the temperature range examined. The thick material was needed to enable the measurement of diffusivity. There have been numerous suggestions that the permeability of PP should follow linear Arrhenius behavior, but to the best of our knowledge a comprehensive data set covering a large temperature range has so far remained elusive. Permeability has been measured between 4 x 10^{-11} to 9 x 10^{-10} ccSTP/cm-s-cmHg at RT, diffusivity between 1.1 x 10^{-8} to 3 x 10^{-7} cm^2/s at RT, and activation energies for P_{ox} of PP have been quoted as 39 kJ/mol (37 kJ/mol for D, implying little contributions from solubility) at 12 to 29°C [64], 48 kJ/mol [65], 45 kJ/mol [66], 49 kJ/mol [67], and 43.1 kJ/mol as an average value between RT and 60°C from an extensive literature review by Francois-Heude [27,28]. Variations are

undoubtedly due some differences in crystallinity and its expected dependence on processing history. An average injection molding PP grade examined here yielded ideal linear Arrhenius behavior for P_{ox} between 25 and 140°C with an E_a of 44 kJ/mol, in perfect agreement with the existing lower temperature data [27,28]. Similarly, our measured data for P_{ox}, D, S at RT fit in the middle of these literature data. At 140°C the material may experience a reduction in crystallinity through the beginning of partial melting, which should enhance permeability, but any such effect is not yet noticeable in the data obtained. Beyond 140°C the material will melt and soften quickly which then requires a different approach to measure its permeative behavior. The solubility of ~ 1 x 10^{-3} cc(STP)/cc-cmHg was found to be approximately steady with temperature, which means that the E_a of D nearly matches that of P_{ox}. The measured P_{ox}, D, S data for PP are included in Figs, 3 to 5. Validation of E_a and excellent Arrhenius behavior up to 140°C provides important feedback for the polymer degradation community dealing with thermal oxidation models for polyolefins [36,38,68-70].

3.5. Other considerations for permeation measurements

3.5.1. Non-Fickian drift component in permeation at elevated temperature

Oxidation during permeation should in principle only reduce equilibrium flux, but not affect diffusivity and time-dependence of the experiment. For most materials when oxidation participates, equilibrium conditions after the major Fickian diffusion response will be obtained quickly. On some occasions, however, we have noticed a weak ongoing non-Fickian upward drift in the final flux. An example is shown in Fig. 10 for the MVK-14 matrix material at 130°C under oxygen. This behavior appears to be more pronounced for O_2 rather than air conditions and was observed when the oxidative loss, based on comparison of air and O_2 permeability in the 80 to 130°C regime, was still relatively low. The reasons for this behavior are currently unknown. Interestingly, at 160°C (Fig. 10) besides an apparent delayed creep component, there is also a significant effect on diffusivity, i.e. the initial rise in flux is significantly delayed. These phenomena could be a reflection of more complicated mechanistic aspects to reach steady oxidation reactions throughout the material or indications that the material oxidation rate increases slightly with oxidation.

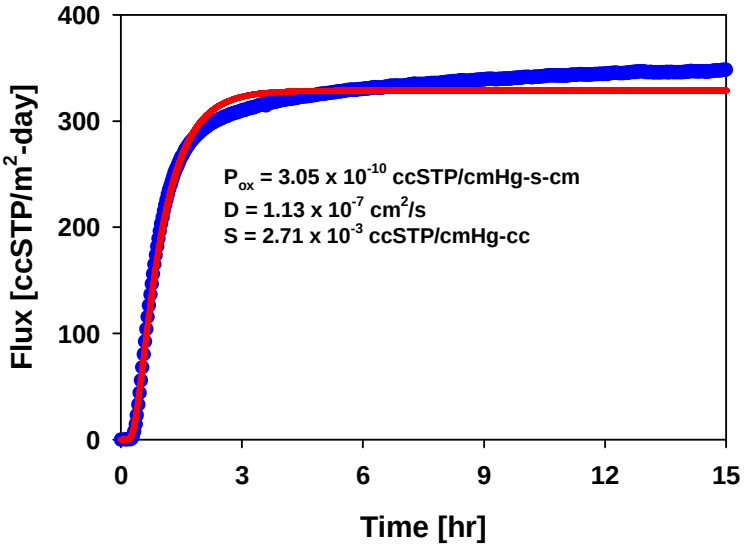

Fig. 10 Example of measured permeative flux and its fit for MVK-14 material for pure O_2 at 630 Torr and 130°C. There is some evidence for an evolving subtle drift in equilibrium (non-Fickian component) for extended times at elevated temperatures.

While non-steady oxidation rates have been observed in the past for some materials (they could drift up or down over time with evolving oxidation level) and such effects will influence permeation experiments, the changes in the extent of oxidation over the course of the experiment here are negligible, and additionally the oxidative loss term (overall flux reduction) was confirmed to be low. Furthermore, this explanation cannot easily account for the delay in the flux increase as the oxygen diffusion time scale is expected to be much longer than the kinetic timescale of free-radical equilibrium, and much shorter than oxidation rate decline behavior with increasing oxidation level. Therefore, subtle changes in the transport properties involved are a more likely. One possible explanation that could be supposed responsible for these anomalies is the existence of a Langmuir sorption [45], yet preliminary Fickian models incorporating a Langmuir term in solubility failed to produce either the delay to rise or the slow drift in final flux. Another more likely explanation may come from the thermodynamic interaction of the gas penetrant (e.g. oxygen) and the polymer chains, as has been considered [46]. This non-Fickian thermodynamic model of gas permeation allows for certain polymeric phenomena (e.g. swelling and plastization) that may very well agree with the experimental data presented here, but further investigation is needed to verify. This is certainly an example where an ideal Fickian diffusion process (e.g. the DMS model) combined with a reactive term does not sufficiently describe the experimental observations and some anomalous behavior develops at high temperatures.

3.5.2. Compositional and absolute air feed pressure variations

Two experiments were conducted to examine the expected proportionality between O_2 partial pressure and permeative flux in terms of potential complications by total pressure or competitive N_2 permeation based on N_2 partial pressure differences. It is important to remember that the carrier gas detector flow is fixed at 98% N_2 at 630 Torr for ABQ. Therefore, variations in total pressure and composition on the supply side do not only

change p_{O2} conditions, but also those for N_2 in the feed, where N_2 permeation (counter permeation in most cases) is not expected to influence the O_2 transfer process.

We first conducted a constant pressure test series using 50 µm Kapton film at 65°C for gas feed compositions of 50/50 air/N_2, air, 50/50 O_2/N_2, and pure O_2 which provided a series of increasing partial pressure for O_2 starting with 100% N_2 at 630 Torr. For these experiments the N_2 partial pressure is lower in the feed than in the N_2 detector flow, hence N_2 is expected to permeate from the detector flow (617 Torr N_2) to the feed gas flow (for example 0 Torr N_2 when pure O_2 is used) as a counter mass transport in comparison with the O_2 permeative direction. P_{ox}, D, S can be determined in two ways, from the increase in flux with time when switching from N_2 to the target O_2 pressure conditions and likewise from the resulting flux decay when switching back to reduced O_2 pressure or 100% N_2 pressure. Fig. 11 shows the result of this compositional up and down series.

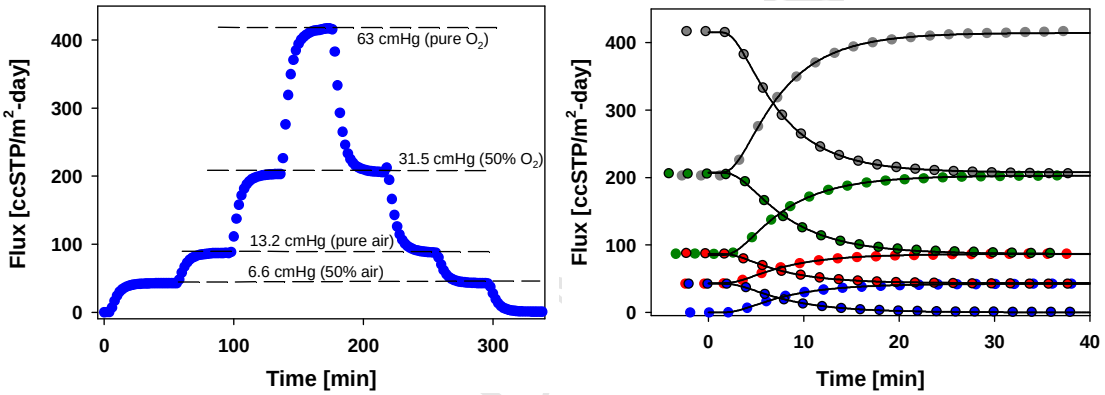

Fig. 11 Example of feed gas compositional changes for O_2 flux through Kapton film (50 µm) at 65°C for different O_2 partial pressures, i.e. compositional variation at 63 cmHg total pressure (O_2 + N_2). The enlarged individual gas switching experiments are shown on the right. These experiments yield consistent permeability (included in Fig. 13) and diffusivity.

A second series used air with increasing pressure, which was achieved by adjusting the feed gas flow with a metering needle valve to the desired pressure condition. Pressures were chosen as 12.18 psi (630 Torr ambient) plus 4, 6, 8, 10, 12, and 14 psi providing p_{O2} from 132, 175, 197, 219 Torr and so on. For these experiments the N_2 conditions changed from 498 to 1070 Torr in the feed gas. Therefore, for most of these conditions, N_2 is expected to permeate into the detector gas flow in parallel with O_2 transport.

Figure 12 shows the equilibrium O_2 flux for all p_{O2} conditions. The underlying average P_{ox} for 1D film permeation can be extracted from this plot by taking the slope (dF/dp_{O2}) and multiplying with thickness. This 'material permeability' was determined as 3.82 x 10^{-11} ccSTP/cm-s-cmHg. It compares well with the individually determined P_{ox} data (Fig. 13), which have very limited scatter as a function of p_{O2} (errors in pressure, composition and flux reading). Similarly, an average D = 8.63 x 10^{-9} cm^2/s and S = 4.40x 10^{-3} cc(STP)/cc-cmHg is determined from these collective experiments.

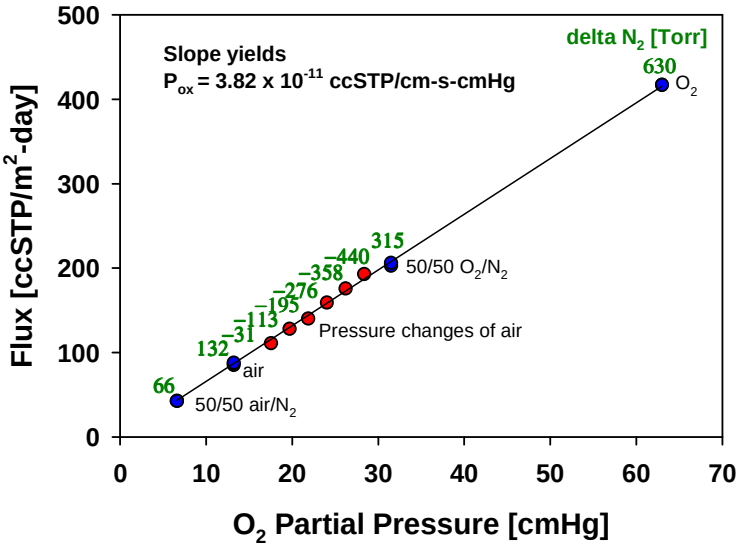

Fig.12 Flux for 50 µm Kapton film at 65°C as a function of absolute O_2 partial pressure, obtained by feed-gas compositional changes and pressure changes of air (ambient O_2 pressure in ABQ equals 13.2 cmHg). Counter (positive N_2 pressure differential with regard to sensor side flow) and parallel N_2 permeation (negative N_2 pressure differential) occurred during these measurements showing that O_2 permeation is completely independent of competing N_2 permeation processes. The absolute N_2 partial pressure difference as pick-up gas (fixed at 63 cmHg) minus feed-gas is noted on each data point. The resulting permeability data have been added to Fig. 13.

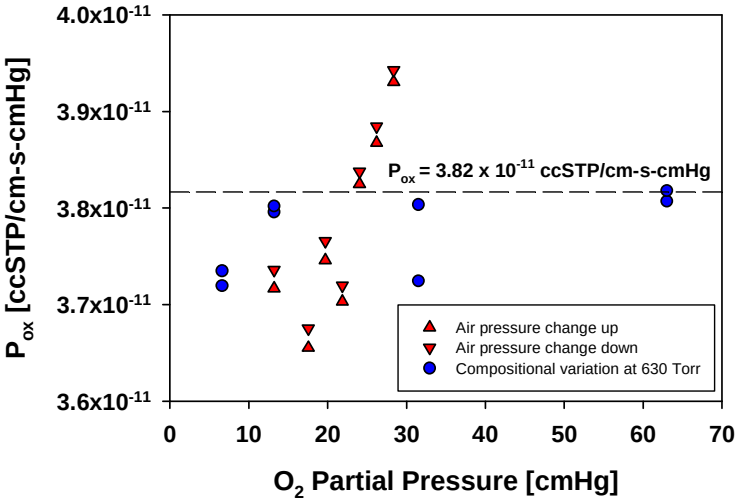

Fig.13 Permeability for a Kapton film (50 µm) at 65°C determined from multiple total pressure (air) and compositional variations at 630 Torr, showing only small variance.

These experiments show that the nitrogen partial pressure condition and associated N_2 permeation direction (parallel or opposing transport) do not influence the O_2 permeation process. A secondary non-Fickian convective mass transport component, which should be pressure dependent, can at least be ruled out for Kapton and is expected to be equally

absent for other materials. These experiments demonstrate that over the accessible pressure regime P_{ox} is independent of pressure. Further, for these conditions there is no oxidative component (chemical loss) due to the linear behavior of this material at lower partial pressures. It is also clear, that elevated pure O_2 pressure can be an avenue to overcome oxidative loss and thickness limiting issues for material characterization.

3.5.3. Intrinsic detector response

As mentioned, O_2 transport from the heated experimental membrane assembly to the detector (~ 3 feet of tubing), and the intrinsic detector behavior represent some delayed response characteristics. Experiments for which equilibrium permeation occurs within less than 10 minutes should be approached with caution for the determination of diffusivity. Meaningful feedback is then limited to 'diffusivity greater than'. An attempt was made to document the intrinsic detector signal decay features, by switching rapidly from a high O_2 reading to a zero condition. This was accomplished by switching from a high O_2 permeation experiment to a carrier gas bypass condition allowing for instant pure N_2 flow to the detector. Fig. 14 shows signal decays on the order of one magnitude within 2 to 3 minutes. This means that changes in the diffusion driven signal faster than that will be convoluted by intrinsic detector response features at least when switching from oxygen rich to poor. Increasing film thickness can help the determination of diffusivity by slowing down the process, but it has to be carefully balanced with oxidation effects, which are normally enhanced for thicker samples.

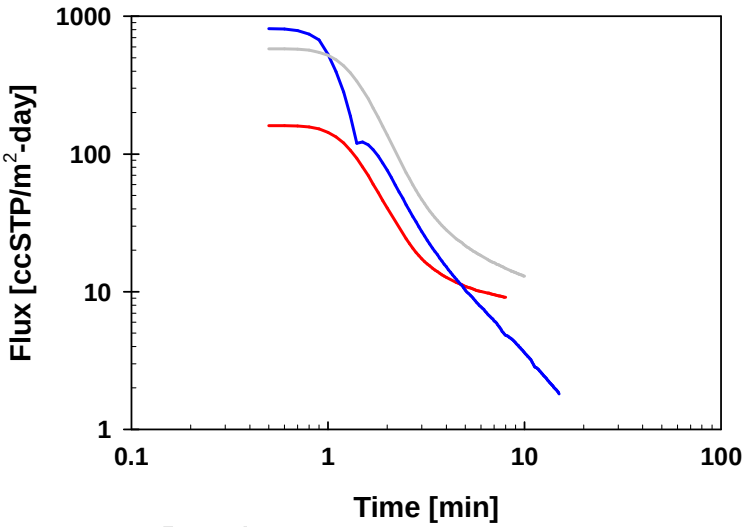

Fig.14 O_2 flux through Kapton polymer film followed by switch to pure N_2 carrier gas (at time zero) achieved by bypassing the external permeation cell. This results in an instantaneous change in the composition of the N_2 pick-up gas flow to the detector and a rapid but delayed decline in detector response. The highest signal decay was acquired over two sensitivity settings given by an automatic instrumental resistor switch (small dip in the blue curve).

3.5.4. DLO conditions as an example for high temperature Kapton film

We discussed earlier that additional high temperature permeability data for the 50 µm Kapton film could be obtained from fast equilibrium flux measurements resulting in a step-like function in the detector response, hence with diffusivity and solubility no longer accessible. Increasing film thickness will reduce flux and slow down the process, but oxidation becomes equally more important. Further, for severe DLO conditions the uncertainties increase and corrections through the reactive transport model are also no longer feasible. This means that for many materials at high temperatures it will not be possible to measure a true 'physical' permeability for oxygen.

For the 50 µm Kapton film the beginning of DLO conditions was observed at 150°C, with model corrections being reasonable up to 230°C. The Arrhenius plot for the experimental permeability at a range of O_2 partial pressures (50% air, air, 50% O_2 and pure O_2) and the corrected *P* obtained using the 'reactive transport model' are included in Fig. 15 which shows linear behavior with an E_a of 22 kJ/mol. We recognize that DLO effects are most important when the O_2 feed partial pressure is low, therefore using pure O_2 can be used as a strategy to minimize oxidation effects as best as possible. Lacking specific data for oxidation rate and β, the model corrections here were accomplished through the correction of permeability (see 'flux correction factor' mentioned earlier) to coalesce to an average value for P_{ox} at all partial pressures at each temperature, and through minimization of scatter in oxidation rate and β by allowing for their own temperature dependence. Having beta with its own temperature dependence reduces scatter better in the determination of the oxidation rate. We do not claim this approach to be perfect, but it shows that suitable corrections can be made and simultaneously offer guidance for the relevant oxidation rate ϕ and β (shown in Fig. 16 with their temperature dependence). While these experiments unquestionably demonstrate oxidation to be important for Kapton starting at ~ 150°C, the origin for this behavior is not clear. Kapton is regarded as a high temperature capable and very stable polymer and has no easily oxidizable aliphatic carbon. This suggests direct oxidation of aromatic and imide ring structures, which of course is mechanistically intriguing and usually regarded as thermally not feasible. We also note that high temperature values for P_{ox} may diverge from published data. For example the Polymer Handbook quotes a value of 2.3×10^{-10} in good agreement with our measured 1.8×10^{-10} ccSTP/cm-s-cmHg at 160°C, with an E_a (135-240°C) of 18.4 kJ/mol in comparison with our ~ 22 kJ/mol [26]. As we have discussed above (Fig. 15), oxidation at higher temperatures is expected to affect E_a and any measured P_{ox}.

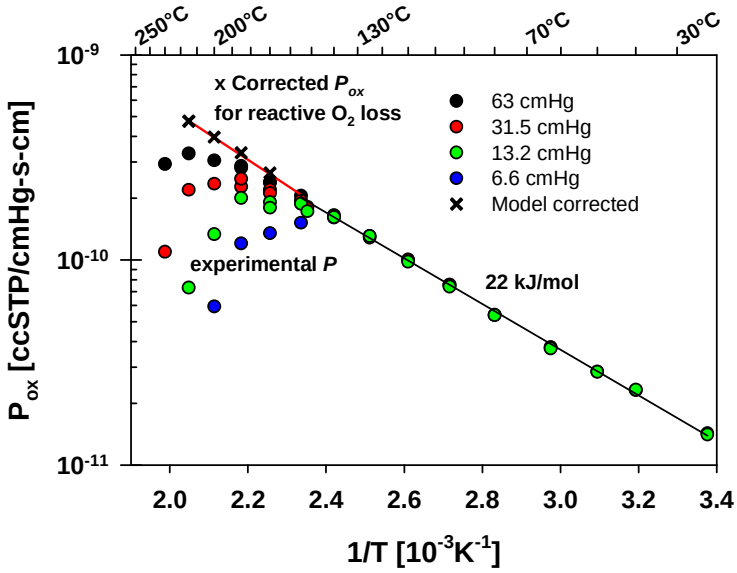

Fig. 15 Permeability for Kapton measured on 50 µm film showing the strong influence of DLO in the 160 to 220°C regime. The underlying material property can be determined using the reactive transport model, which enables corrections for oxidative loss.

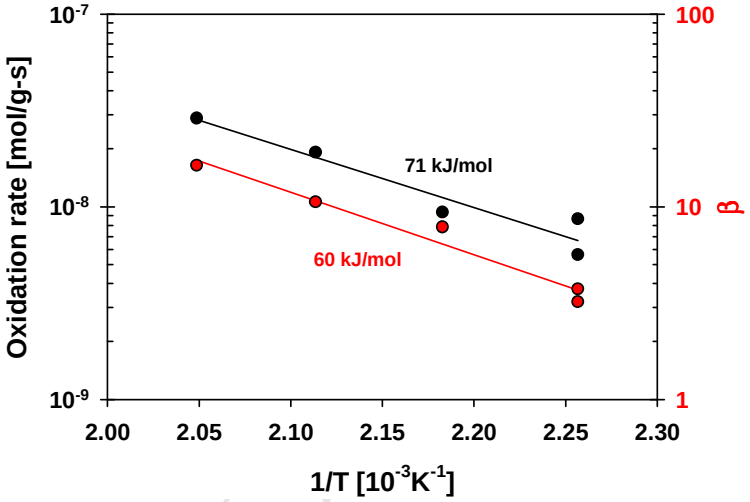

Fig. 16 The large data set of *P* taken for different partial pressures in Fig. 15 can be corrected for oxidation with the reactive transport model, which in parallel provides guidance on underlying oxidation rate and β.

4. Conclusions

A commercial instrument was customized to enable well resolved time-dependent transport behavior through polymer films at elevated temperature thereby yielding data for P_{ox}, D and S which was not possible with previous instrumentation [13]. Experimental conditions were optimized based on the given dynamic detector sensitivity, the dimensions of an external stage to hold small samples, and chosen film thickness to

offer a suitable regime for diffusion and permeation measurements (i.e. before intrinsic detector delay interferes with rapid time-response measurements). Primary flux measurements were obtained for multiple materials, including epoxy films at multiple O_2 partial pressures. This approach allowed assessing the extent of any oxidative loss due to oxidation during the experiment and verified that the true physical permeation behavior was measured when possible.

Experimental flux curves as time dependent mass transport through the films were fitted with a Fickian diffusion model which allowed the permeability, diffusivity and solubility constants to be determined. In high temperature situations where physical transport competes with reactive oxidative loss, a diffusion limited oxidation model was used to determine permeability either by using known oxidation rates, or through parallel fits for multiple partial pressures to yield a constant oxidation rate. This allowed permeability, oxidation rates and β to be extracted where possible.

For most materials excellent linear Arrhenius behavior is observed for permeability and diffusivity. As anticipated, solubility does not depend much on temperature (low E_a) and trends only slightly lower with increasing temperature below T_g. As summarized in Table 1 permeability was determined in the range of ~ 1 x 10^{-11} to 1 x 10^{-8} ccSTP/ cm-s-cmHg with activation energies in the range of 11 kJ/mol for MVK-14 to 75 kJ/mol for an epoxy (828/D230) above T_g. Diffusivity was determined between ~ 1 x 10^{-9} to 1 x10^{-5} cm^2/s with E_a in the range of 32 kJ/mol for MVK-14 to 59 kJ/mol for epoxy (828/D400). Solubility was in the range of ~ 0.9 x 10^{-3} to 2 x 10^{-3} ccSTP/cc-cmHg with E_a between -22 kJ/mol for epoxy (828/D400) to 3 kJ/mol for PP. For all measurements, film thickness and to a lesser degree film size, as well as oxidative loss and maximum flux (to avoid signal overload) had to be accommodated. There is an upper limit for the measurement of diffusivity based on the intrinsic detector behavior for this instrument, as well as for permeability, neither of which is easily measured using thicker films at higher temperatures, as the reactive loss of oxygen becomes more dominant. Since polymer oxidation competes with permeation, it is also clear that basic O_2 transmission rates [8], particularly when measured at elevated temperatures, for many materials will not inversely multiply with thickness. Any calculation of transmission rate for a thicker specimen will constitute a maximum value since competitive oxidation will by default reduce its rate, hence permeation rates will only offer guidance as boundary conditions.

Table 1: Summary of P_{ox}, D, S data obtained in this study. These data were taken at minimum as an average of 4 measurements for air and O_2 with up and down repeats for flux as shown in Fig. 1. Note: Data were not always taken at identical temperatures with some taken at plus (a) or minus 5°C (b) from the temperature denoted in the column (i.e. *P* for MVK-14 for '125°C' relates to 120°C and for '95°C' to an actual temperature of 100°C.)

Permeability [ccSTP/cm-s-cmHg]	25°C	40°C	50°C	65°C	80°C	95°C	110°C	125°C	140°C
828/A2049	1.40E-11	2.40E-11	3.30E-11	5.10E-11	7.70E-11	1.20E-10	1.60E-10	2.40E-10	3.10E-10
828/D230	7.53E-12	1.27E-11	1.62E-11	2.47E-11	4.49E-11	1.15E-10	3.03E-10	6.02E-10	1.06E-09
828/D400	7.26E-12	1.65E-11	3.28E-11	9.17E-11	2.26E-10		9.87E-10	1.49E-09[b]	
Kapton	1.43E-11	2.32E-11	2.85E-11	3.88E-11	5.39E-11	7.51E-11	9.94E-11	1.30E-10	1.63E-10
MVK-14	7.10E-11		1.16E-10		1.88E-10	2.60E-10[a]		3.03E-10[b]	4.28E-10
Polypropylene	1.97E-10	6.59E-10	9.38E-10	2.02E-09	3.44E-09	6.47E-09	1.23E-08	1.68E-08[b]	
Diffusivity [cm^2/s]									
828/A2049	4.97E-09	1.01E-08	1.67E-08	3.28E-08	5.22E-08	7.66E-08			
828/D230	2.92E-09	5.84E-09	1.17E-08	2.56E-08	5.48E-08	1.20E-07[a]			
828/D400	5.36E-09	1.69E-08	3.47E-08	8.88E-08	1.90E-07	2.87E-07[b]	5.37E-07		
Kapton	1.19E-09	2.79E-09	4.36E-09	7.23E-09	1.49E-08				
MVK-14	4.97E-09		1.46E-08		3.97E-08	6.86E-08[a]		1.12E-07[b]	1.97E-07
Polypropylene	2.12E-07	6.05E-07	9.70E-07	1.88E-06	3.29E-06	5.77E-06	1.29E-05	1.48E-05[a]	
Solubility [ccSTP/cc-cmHg]									
828/A2049	2.82E-03	2.28E-03	1.92E-03	1.55E-03	1.44E-03	1.57E-03			
828/D230	2.72E-03	2.18E-03	1.39E-03	9.59E-04	8.62E-04	1.55E-03[a]			
828/D400	1.36E-03	9.73E-04	9.45E-04	1.03E-03	1.19E-03	1.24E-03[b]	1.84E-03		
Kapton	1.20E-02	8.28E-03	6.54E-03	5.19E-03	3.61E-03				
MVK-14	1.43E-02		7.94E-03		4.74E-03	3.79E-03[a]		2.70E-03[b]	2.18E-03
Polypropylene	9.34E-04	1.09E-03	9.70E-04	1.08E-03	1.05E-03	1.12E-03	1.07E-03	1.46E-03[a]	

Interestingly, any speculation or perhaps expectations that T_g should be noticeable in an Arrhenius plot of diffusivity could not be confirmed in this study. Instead, a transition in solubility was observed for two epoxy materials where T_g was in the middle of the temperature range that could be examined. This means T_g is apparent in a transition for permeability with temperature, but its origin is through solubility and not T_g related changes in diffusivity (see overview for this behavior in Fig. 17 for the 828/D230 and 828/D400 epoxy materials). The computationally smoothed derivative in the P_{ox} Arrhenius plot as temperature dependent E_a shows nicely how T_g coincides with the steepest transition and highest E_a (see Fig. 17 b and c). Such a behavior is consistent with free-volume changes at T_g affecting primarily solubility, but not the molecular interactions (chemical affinity) between the polymer and oxygen which governs diffusivity. A similar observation for water transport phenomena has been discussed where the diffusion coefficient does not vary significantly with nanopore size or volume fraction [71,72]. However, there could be exceptions involving permeants and matrix materials capable of significant hydrogen bonding. In this case, traversing the glass transition might be expected to occur in parallel with disruption of hydrogen bonding behavior and hence more pronounced local mobility changes. Further, there is also consensus that high free-volume glassy polymers can be viewed as micro-porous materials [73] as studied by PALS [74] and that the free volume size increases above T_g, but that the hole concentration (number of holes) does not change [75]. This implies that the diffusional path length between free-volume sites does not necessarily experience a change at T_g. While overall diffusional mobility will increase with temperature, there appears to be no influence on diffusivity by a sudden increase in free-volume hole size in contrast to the Cohen-Turnbull model which predicts that diffusion coefficients increase strongly as free volume increases [48]. . However, larger holes sizes are expected to enable higher penetrant solubility as has been observed in this study. An alternative perspective is offered by the usual relaxation times and mobility which can be probed by NMR in the glassy and rubbery state. In the glass there are local segmental fluctuations

on the order of picoseconds, but the displacement for these limited vibrations (mean square collision diameter) is limited. In the rubbery regime motions will occur towards the micro and millisecond time scales that produce a significant motional averaging, meaning the mean squared displacement is large. Self-diffusion changes by several orders of magnitude when transitioning T_g, and it is common to describe D in the rubbery state on the order of 10^{-9} versus 10^{-17} cm^2/s in the glassy state [76]. Considering that our measured diffusivities are orders of magnitude faster than self-diffusion in the glassy state speaks for the fact that the observed diffusion behavior for O_2 is strongly decoupled from the motions present in the glassy state. This suggests that additional mobility occurring at Tg will in turn also have little influence on the O_2 diffusion process, because the interaction of this simple gas with the polymer is always weak. However, it is likely that larger penetrant molecules that more strongly interact with the polymer chain through polar interactions will be more susceptible to transitions at T_g [77].

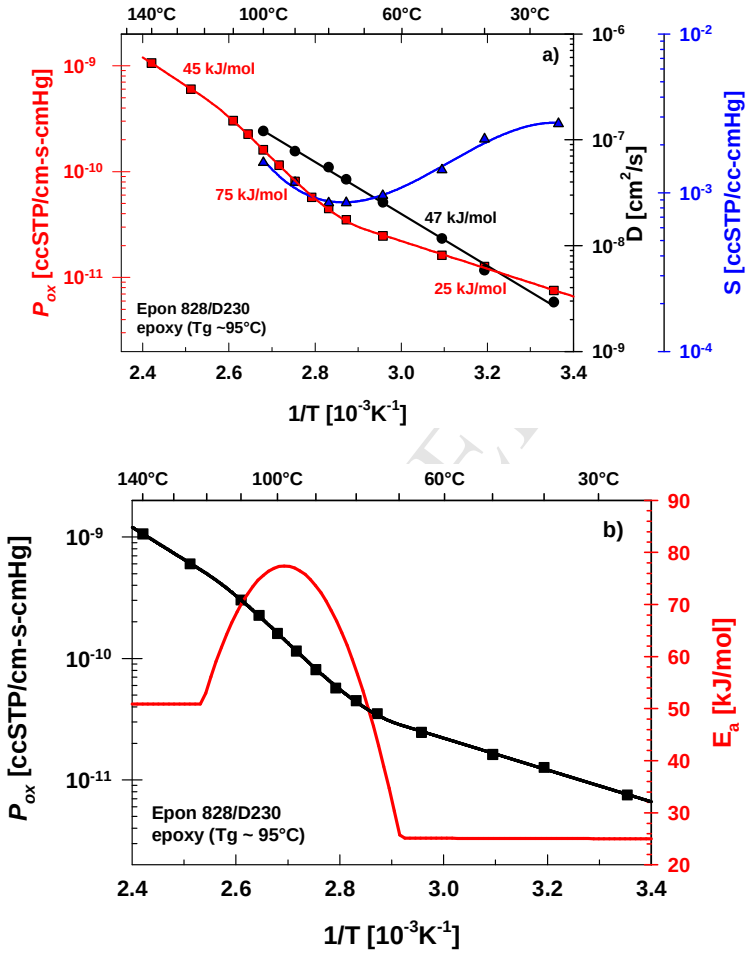

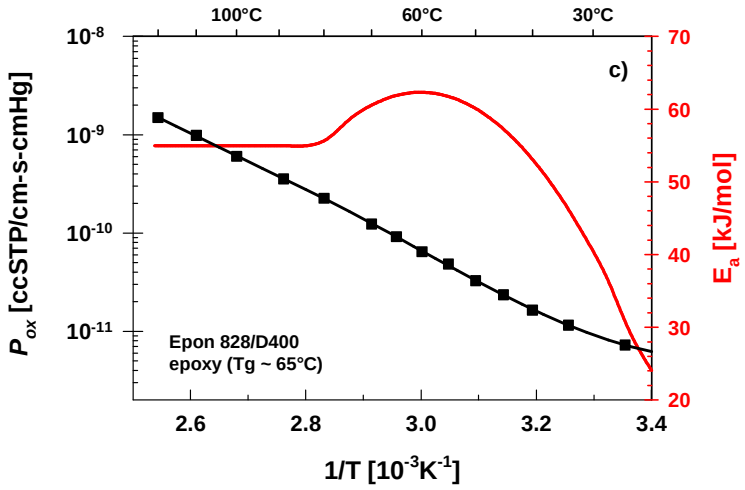

Fig.17 Overview of the effects of T_g on O_2 permeability. a) Plot for 828/D230 showing that a transition in solubility is the origin for the transition in P_{ox}. Permeability and its temperature dependent E_a (derivative in the Arrhenius plot) for 828/D230 (b) and 828/D400 (c).

The following permeative polymer characterization was achieved:

- Novel material characterization for the determination of P_{ox}, D, and S for O_2 transport was documented for epoxies and similar polymers/thermosets.
- A numerical solution approach for fitting flux responses was applied for the determination of diffusivity.
- A mathematical model coupling physical diffusion with reactive O_2 loss was developed and applied to accommodate oxidation during permeation measurements and obtain corrected P data where applicable.
- The effects of diffusion-limited oxidation (DLO) as a flux correction factor due to reactive O_2 loss were shown for epoxy or Kapton materials at high temperatures.
- No influence whatsoever of N_2 on O_2 permeation behavior was observed either under parallel or counter flow conditions.
- Under non-oxidative conditions permeability showed excellent linearity with O_2 partial pressure variations.
- The T_g for two epoxy materials was found to affect solubility rather than diffusivity.

Outstanding issues and forward-looking efforts:

- The 'reactive diffusion model' can yield P_{ox} and D for moderate oxidative conditions, but the lower boundary (oxidative competition) of this model is not clearly established. We estimate that under severe oxidative conditions (flux correction factor less than ~ 0.2) the material behavior is too convoluted for meaningful data analysis.
- The origin of some creep, i.e. anomalous non-Fickian behavior for flux at elevated temperature is not well understood. Interestingly, this effect is more pronounced under pure O_2 conditions, where oxidative reduction in total flux should be less important. Subtle creep may be due to thermodynamic swelling

and plasticization effects from the interaction of oxygen with the polymer chains at high temperatures representing an evolving additional activity term for dissolved O_2.

- There is some evidence for an unexpected delay in Fickian diffusion for thick epoxy materials even at moderate temperatures suggesting the initial O_2 ingress is more affected by oxidation than the current 'reactive diffusion' model predicts. Reduced local O_2 concentrations due to oxidation in the early stage of the permeation experiment may not allow Fickian diffusion to develop immediately. This is reminiscent of an early non-Fickian sorption process or more effective oxidative loss than the current auto-oxidation model would predict.
- All trends here have shown that diffusivity does not transition with T_g, yet the exact mechanistic origin for this lack of sensitivity is not clear. The influence of T_g on O_2 diffusion phenomena needs further investigation to corroborate these observations.

Acknowledgments

We gratefully acknowledge the BMI and MVK-14 samples from K. Pochiraju and G. Tandon. Sandia National Laboratories is a multi-mission laboratory managed and operated by National Technology and Engineering Solutions of Sandia, LLC, a wholly owned subsidiary of Honeywell International, Inc., for the U.S. Department of Energy's National Nuclear Security Administration under contract DE-NA0003525. Note: The views expressed in this article do not necessarily represent the views of the U.S. Department of Energy or the United States Government.

References

[1] Duncan B. Review of Measurement and Modelling of Permeation and Diffusion in Polymers, 2005, NPL Report DEPC MPR 012, pp 68.

[2] Muller K. Faster results. *Kunststoffe* 2011;101:75.

[3] Maxwell AS. Review of Data on Gas Migration through Polymer Encapsulants, 2008, SERCO/TAS/000500/001, pp 50.

[4] Buntinx M, Willems G, Knockaert G, Adons D, Yperman J, Carleer R, Peeters R. Evaluation of the thickness and oxygen transmission rate before and after thermoforming mono- and multi-layer sheets into trays with variable depth. *Polymers* 2014;6:3019.

[5] Khoe C, Chowdhury S, Bhethanabotla VR, Sen R. Measurement of oxygen permeability of epoxy polymers. *ACI Mater J* 2010;107:138.

[6] Khoe C, Sen R, Bhethanabotla VR. Oxygen Permeability of Fiber-Reinforced Polymers. *J Compos Constr* 2011;15:513.

[7] Flaconneche B, Martin J, Klopffer MH. Transport properties of gases in polymers: Experimental methods. *Oil Gas Sci Technol* 2001;56:245.

[8] ASTM Standard D 3985-81; Oxygen gas transmission rate through plastic film and sheeting using a coulometric sensor, Annual Book of ASTM Standards 15.09, 1999, pp

[9] Yekta A, Masoumi Z, Winnik MA. Luminescence measurements of oxygen permeation and oxygen diffusion in thin polymer films. *Can J Chem* 1995;73:2021.
[10] Rharbi Y, Yekta A, Winnik MA. A Method for Measuring Oxygen Diffusion and Oxygen Permeation in Polymer Films Based on Fluorescence Quenching. *Anal Chem* 1999;71:5045.
[11] Murphy TM, Freeman BD, Paul DR. Physical aging of polystyrene films tracked by gas permeability. *Polymer* 2013;54:873.
[12] Rutherford SW, Limmer DT, Smith MG, Honnell KG. Gas transport in ethylene-propylene-diene (EPDM) elastomer: Molecular simulation and experimental study. *Polymer* 2007;48:6719.
[13] Celina M, Gillen KT. Oxygen Permeability Measurements on Elastomers at Temperatures up to 225°C. *Macromolecules* 2005;38:2754.
[14] Celina MC. Review of polymer oxidation and its relationship with materials performance and lifetime prediction. *Polym Degrad Stab* 2013;98:2419.
[15] Verdu J. Oxidative ageing of polymers. Hoboken: ISTE Ltd and John Wiley & Sons Inc, 2012.
[16] Colin X, Verdu J. Aging of organic matrix composite materials. In:Nicolais L, Borzacchiello A, Lee SM, eds. Wiley Encyclopdia of Composites (2nd Ed). 2012, p 35.
[17] Audouin L, Langlois V, Verdu J, de Bruijn JCM. Role of oxygen diffusion in polymer aging: kinetic and mechanical aspects. *J Mater Sci* 1994;29:569.
[18] Audouin L, Gueguen V, Tcharkhtchi A, Verdu J. "Close Loop" mechanistic schemes for hydrocarbon polymer oxidation. *J Polym Sci, Part A: Polym Chem* 1995;33:921.
[19] Gillen KT, Clough RL. Rigorous experimental confirmation of a theoretical model for diffusion-limited oxidation. *Polymer* 1992;33:4358.
[20] Gillen KT, Wise J, Clough RL. General solution for the basic autoxidation scheme. *Polym Degrad Stab* 1995;47:149.
[21] Wise J, Gillen KT, Clough RL. Quantitative model for the time development of diffusion-limited oxidation profiles. *Polymer* 1997;38:1929.
[22] Quintana A, Celina MC. Overview of DLO modeling and approaches to predict heterogeneous oxidative polymer degradation. *Polym Degrad Stab* 2018;149:173.
[23] Cunliffe AV, Davis A. Photo-oxidation of thick polymer samples- Part II: The influence of oxygen diffusion on the natural and artificial weathering of polyolefins. *Polym Degrad Stab* 1982;4:17.
[24] Massey LK. Permeability Properties of Plastics and Elastomers: A Guide to Packaging and Barrier Materials. Norwich, NY 13815: Plastics Design Library / William Andrew Publishing, 2003.
[25] Van Krevelen DW. Properties Determining Mass Transfer in Polymeric Systems. In: Properties of Polymers. Amsterdam, Elsevier, 1997.
[26] Pauly S. Polymer Handbook. In:Brandrup J, Immergut EH, Grulke EA, eds. New York, John Wiley & Sons, Inc., 1999, p 543.
[27] Francois-Heude A, Richaud E, Guinault A, Desnoux E, Colin X. Impact of oxygen transport properties on the kinetic modeling of polypropylene thermal oxidation. II. Effect of oxygen diffusivity. *J Appl Polym Sci* 2015;132:41562/1.

[28] Francois-Heude A, Richaud E, Guinault A, Desnoux E, Colin X. Impact of oxygen transport properties on polypropylene thermal oxidation, part 1: Effect of oxygen solubility. *J Appl Polym Sci* 2015;132:41441/1.
[29] Pochiraju KV, Tandon GP, Schoeppner GA, eds. Long-Term Durability of Polymeric Matrix Composites. Springer Science + Business Media, 2011.
[30] Pochiraju KV. Modeling Thermo-Oxidative Aging and Degradation of Composites. In:Pochiraju KV, Tandon GP, Schoeppner GA, eds. Long-Term Durability of Polymeric Matrix Composites. Springer Science + Business Media, 2011, p 383.
[31] Richaud E, Colin X, Monchy-Leroy C, Audouin L, Verdu J. Diffusion-controlled radiochemical oxidation of bisphenol A polysulfone. *Polym Int* 2011;60:371.
[32] Wise J, Gillen KT, Clough RL. An ultrasensitive technique for testing the Arrhenius extrapolation assumption for thermally aged elastomers. *Polym Degrad Stab* 1995;49:403.
[33] Celina M, Graham AC, Gillen KT, Assink RA, Minier LM. Thermal degradation studies of a polyurethane propellant binder. *Rubber Chem Technol* 2000;73:678.
[34] Gillen KT, Bernstein R, Celina M. Challenges of accelerated aging techniques for elastomer lifetime predictions. *Rubber Chem Technol* 2015;88:1.
[35] Le Gac PY, Celina M, Roux G, Verdu J, Davies P, Fayolle B. Predictive ageing of elastomers: Oxidation driven modulus changes for polychloroprene. *Polym Degrad Stab* 2016;130:348.
[36] Rincon-Rubio LM, Colin X, Audouin L, Verdu J. A theoretical model for the diffusion-limited thermal oxidation of elastomers at medium temperatures. *Rubber Chem Technol* 2003;76:460.
[37] Celina MC, Dayile AR, Quintana A. A perspective on the inherent oxidation sensitivity of epoxy materials. *Polymer* 2013;54:3290.
[38] Rincon-Rubio LM, Fayolle B, Audouin L, Verdu J. A general solution of the closed-loop kinetic scheme for the thermal oxidation of polypropylene. *Polym Degrad Stab* 2001;74:177.
[39] Celina M, Clough RL, Jones GD. Initiation of polymer degradation via transfer of infectious species. *Polym Degrad Stab* 2006;91:1036.
[40] Colin X, Marais C, Verdu J. Thermal oxidation kinetics for a poly(bismaleimide). *J Appl Polym Sci* 2001;82:3418.
[41] Colin X, Marais C, Verdu J. Kinetic modelling and simulation of gravimetric curves: application to the oxidation of bismaleimide and epoxy resins. *Polym Degrad Stab* 2002;78:545.
[42] Colin X, Verdu J. Mechanisms and Kinetics of Organic Matrix Thermal Oxidation. In:Pochiraju KV, Tandon GP, Schoeppner GA, eds. Long-Term Durability of Polymeric Matrix Composites. Springer Science + Business Media, 2011, p 311.
[43] Putthanarat S, Tandon GP, Schoeppner GA. Influence of aging temperature, time, and environment on thermo-oxidative behavior of PMR-15: nanomechanical characterization. *J Mater Sci* 2008;43:6714.
[44] Ju ST, Duda JL, Vrentas JS. Influence of temperature on the diffusion of solvents in polymers above the glass transition temperature. *Ind Eng Chem Prod Res Dev* 1981;20:330.

[45] Vieth WR, Howell JM, Hsieh JH. Dual sorption theory. *J Membr Sci* 1976;1:177.
[46] Minelli M, Sarti GC. Elementary prediction of gas permeability in glassy polymers. *J Membr Sci* 2017;521:73.
[47] Masaro L, Zhu XX. Physical models of diffusion for polymer solutions, gels and solids. *Prog Polym Sci* 1999;24:731.
[48] Sanders DF, Smith ZP, Guo R, Robeson LM, McGrath JE, Paul DR, Freeman BD. Energy-efficient polymeric gas separation membranes for a sustainable future: A review. *Polymer* 2013;54:4729.
[49] ASTM Standard D 792-91; Density and specific gravity of plastics by displacement, Annual Book of ASTM Standards 08.01, 1991, pp
[50] Celina M, Gillen KT, Wise J, Clough RL. Anomalous aging phenomena in a crosslinked polyolefin cable insulation. *Radiat Phys Chem* 1996;48:613.
[51] Mensitieri G, Del Nobile MA, Monetta T, Nicodemo L, Bellucci F. The effect of film thickness on oxygen sorption and transport in dry and water-saturated Kapton polyimide. *J Membr Sci* 1994;89:131.
[52] Sroog CE. Polyimides. *Prog Polym Sci* 1991;16:561.
[53] Tungare AV, Martin GC. Glass transition temperatures in bismaleimide-based resin systems. *Polym Eng Sci* 1993;33:614.
[54] Hopewell JL, George GA, Hill DJT. Quantitative analysis of bismaleimide-diamine thermosets using near infrared spectroscopy. *Polymer* 2000;41:8221.
[55] Hopewell JL, George GA, Hill DJT. Analysis of the kinetics and mechanism of the cure of a bismaleimide-diamine thermoset. *Polymer* 2000;41:8231.
[56] Wunderlich B. Thermal Analysis of Polymeric Materials. Berlin Heidelberg: Springer-Verlag, 2005.
[57] Michaels AS, Bixler HJ. Solubility of gases in polyethylene [and rubbery polymers]. *J Polym Sci* 1961;50:393.
[58] Michaels AS, Bixler HJ. Flow of gases through polyethylene [and rubbery polymers]. *J Polym Sci* 1961;50:413.
[59] Crank J. The Mathematics of Diffusion. 2d Ed. New York: Oxford University Press, 1975.
[60] Minelli M, Sarti GC. Gas transport in glassy polymers: prediction of diffusional time lag. *Membranes* 2018;8:8/1.
[61] Rutherford SW. Polymer permeability and time lag at high concentrations of sorbate. *J Membr Sci* 2001;183:101.
[62] Meares P. The diffusion of gases through polyvinyl acetate. *J Am Chem Soc* 1954;76:3415.
[63] Colin X, Verdu J. Strategy for studying thermal oxidation of organic matrix composites. *Comp Sci Tech* 2005;65:411.
[64] Beltrame PL, Citterio C, Testa G, Seves A. Oxygen permeation through films of compatibilized polypropylene/polyamide 6 blends. *J Appl Polym Sci* 1999;74:1941.
[65] Kiryushkin SG, Shlyapnikov YA. Diffusion-controlled polymer oxidation. *Polym Degrad Stab* 1989;23:185.
[66] Somlai LS, Liu RYF, Landoll LM, Hiltner A, Baer E. Effect of orientation on the free volume and oxygen transport of a polypropylene copolymer. *J Polym Sci, Part B Polym Phys* 2005;43:1230.

[67] Kurek M, Klepac D, Scetar M, Galic K, Valic S, Liu Y, Yang W. Gas barrier and morphology characteristics of linear low-density polyethylene and two different polypropylene films. *Polym Bull* 2011;67:1293.
[68] Richaud E, Farcas F, Bartolomeo P, Fayolle B, Audouin L, Verdu J. Effect of oxygen pressure on the oxidation kinetics of unstabilized polypropylene. *Polym Degrad Stab* 2006;91:398.
[69] Francois-Heude A, Richaud E, Desnoux E, Colin X. Influence of temperature, UV-light wavelength and intensity on polypropylene photothermal oxidation. *Polym Degrad Stab* 2014;100:10.
[70] Francois-Heude A, Richaud E, Desnoux E, Colin X. A general kinetic model for the photothermal oxidation of polypropylene. *J Photochem Photobiol, A* 2015;296:48.
[71] Soles CL, Yee AF. A discussion of the molecular mechanisms of moisture transport in epoxy resins. *J Polym Sci, Part B: Polym Phys* 2000;38:792.
[72] Soles CL, Chang FT, Gidley DW, Yee AF. Contributions of the nanovoid structure to the kinetics of moisture transport in epoxy resins. *J Polym Sci, Part B: Polym Phys* 2000;38:776.
[73] Rutherford SW. Mechanism of sorption and diffusion in a high free-volume polymer. *Ind Eng Chem Res* 2001;40:1370.
[74] Rey L, Galy J, Sautereau H, Simon GP, Cook WD. PALS free volume and mechanical properties in dimethacrylate-based thermosets. *Polym Int* 2004;53:557.
[75] Zhang HJ, Sellaiyan S, Kakizaki T, Uedono A, Taniguchi Y, Hayashi K. Effect of Free-Volume Holes on Dynamic Mechanical Properties of Epoxy Resins for Carbon-Fiber-Reinforced Polymers. *Macromolecules* 2017;50:3933.
[76] Ramesh N, Duda JL. Diffusion in polymers below the glass transition temperature: comparison of two approaches based on free volume concepts. *Korean J Chem Eng* 2000;17:310.
[77] Karlsson OJ, Stubbs JM, Karlsson LE, Sundberg DC. Estimating diffusion coefficients for small molecules in polymers and polymer solutions. *Polymer* 2001;42:4915.

Figures

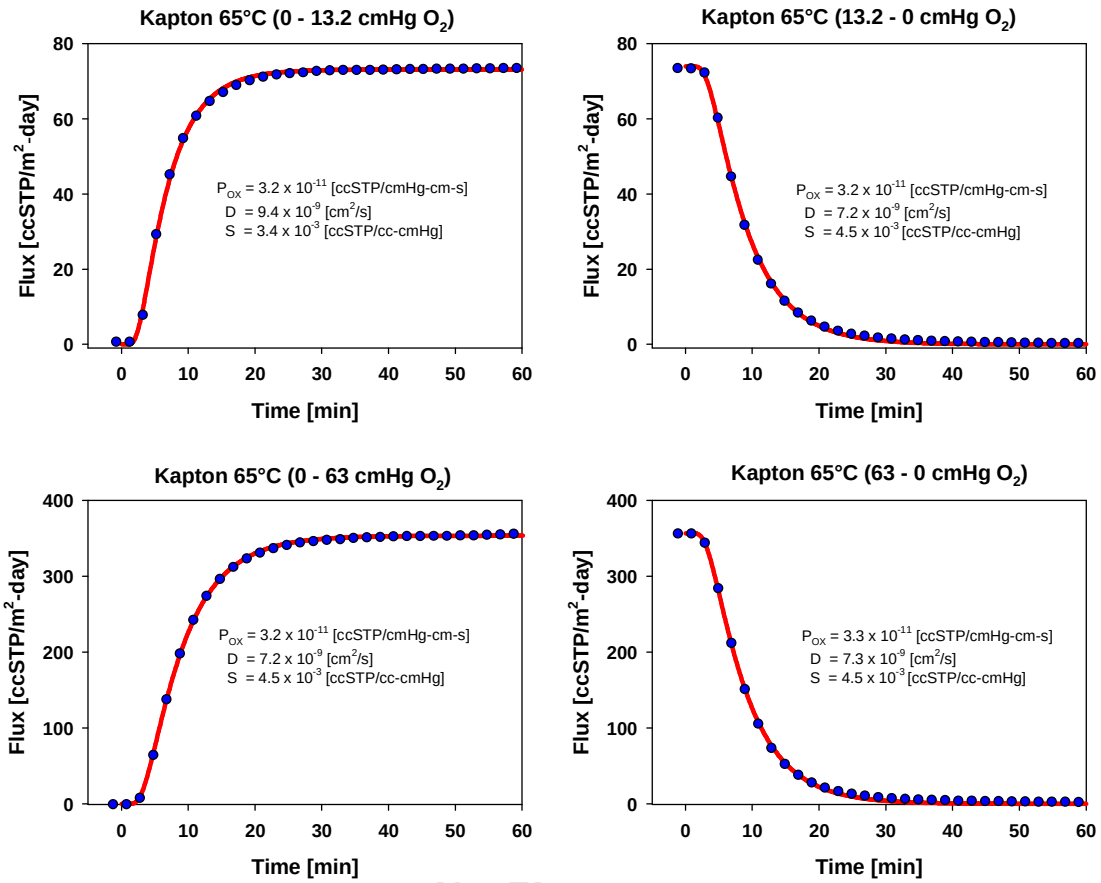

Fig. 1 Flux measurements under air and O_2 conditions for a 50 µm thick Kapton film. These yield *P*, *D*, *S* data when fitted with a Fickian diffusion model (solid line through the experimental data).

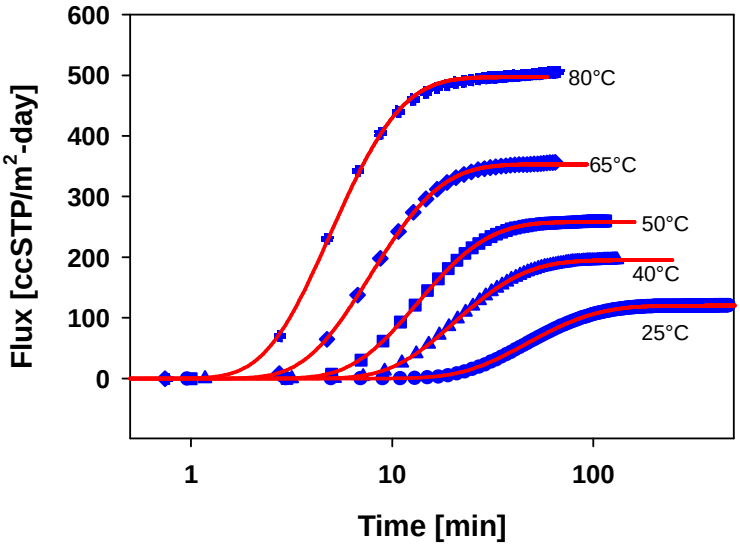

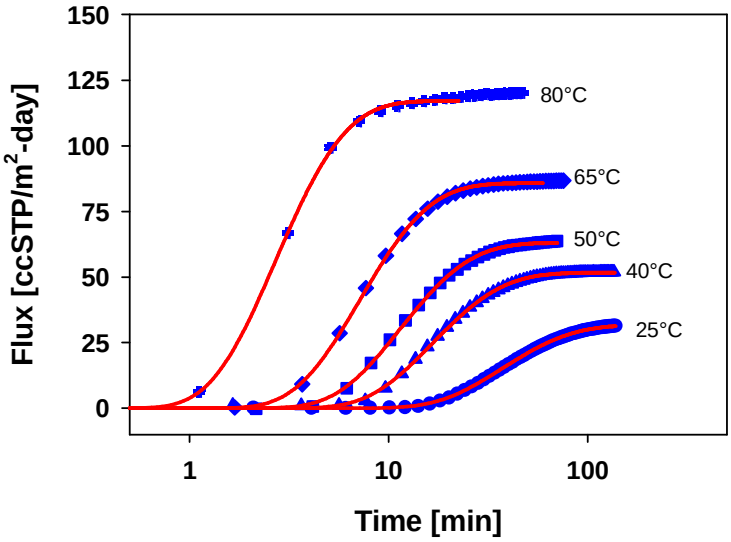

Fig.2 Flux measurements with temperature for a 50 µm Kapton film for pure O_2 (0 to 63 cmHg, upper figure) and under air (0 to 13.2 cmHg, lower figure), both fitted with a Fickian diffusion model (solid line through the experimental data).

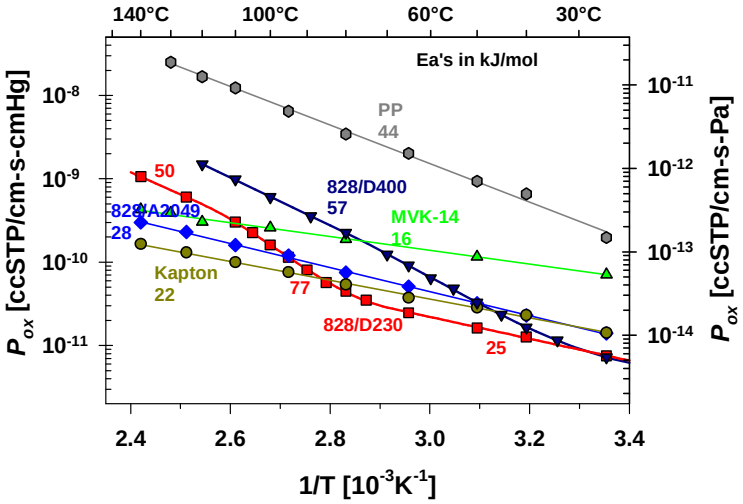

Fig. 3 Arrhenius plot for permeability (P_{ox}) of Kapton, MVK-14, Epoxies 828/A2049, 828/D230, 828/D400 and PP. E_a's range from 11 to 77 kJ/mol as indicated on slopes.

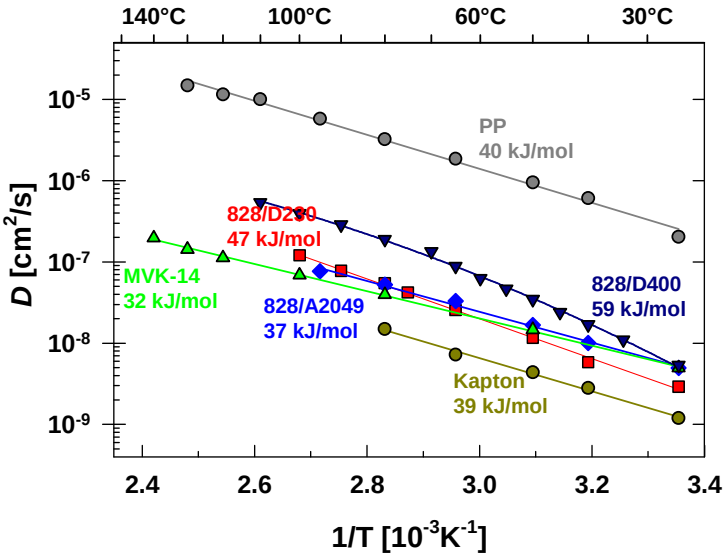

Fig. 4 Arrhenius plot for diffusivity (*D*) of Kapton, MVK-14, Epoxies 828/A2049, 828/D230, 828/D400 and PP.

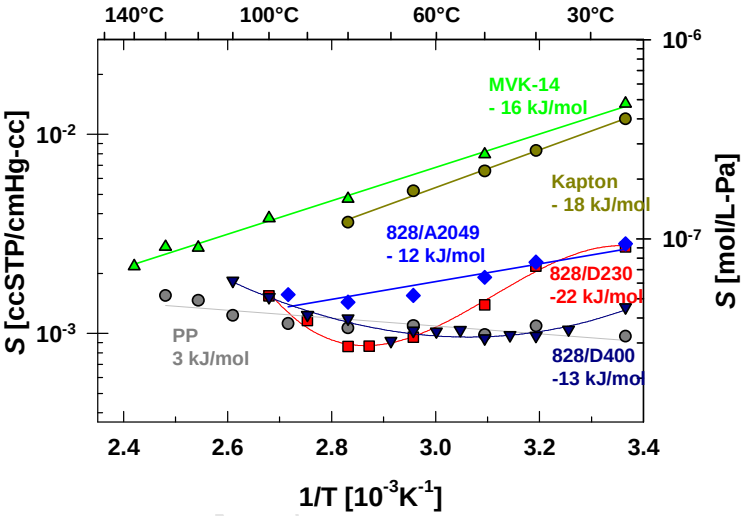

Fig. 5 Arrhenius plot for solubility (*S*) of Kapton, MVK-14, Epoxies 828/A2049, 828/D230, 828/D400 and PP.

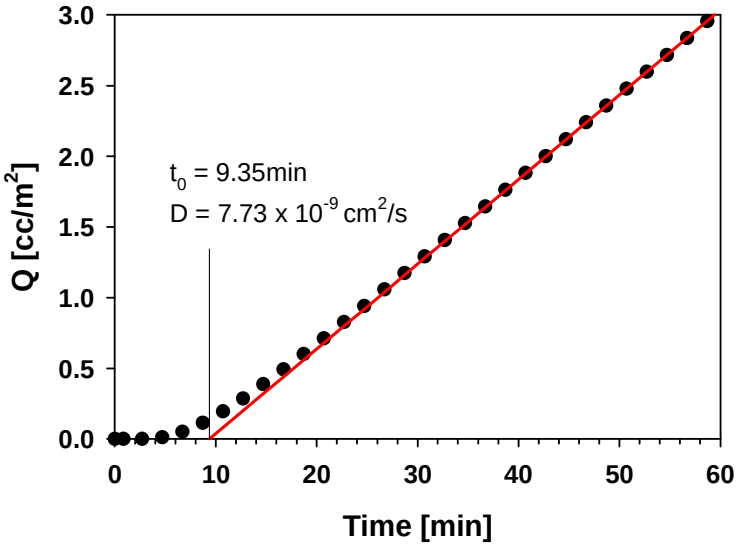

Fig. 6 Traditional time-lag method for determination of *D* from the integrated flux for Kapton at 65°C (air).

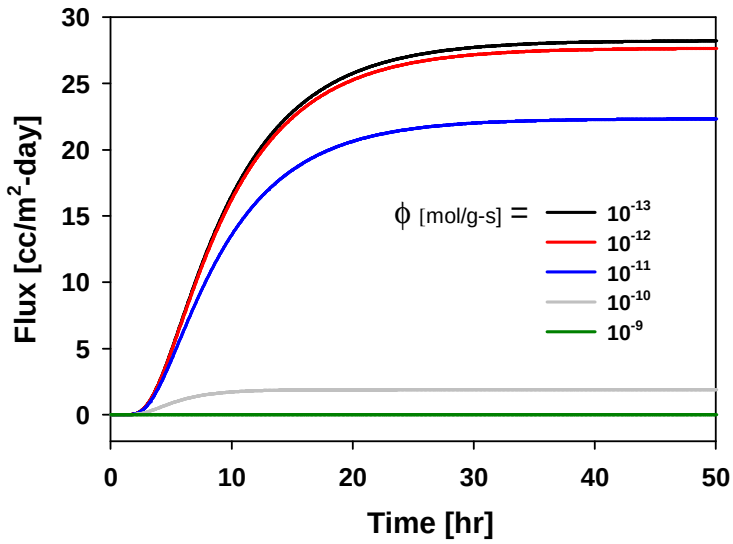

Fig. 7 Reduction in flux with increasing oxidation rate for pure O_2 conditions for a simulated 500 µm thick BMI material at 80 °C. Parameters are P_{ox} = 2.6 x 10^{-11} ccSTP/cm-s-cmHg, *D* = 1.1 x 10^{-8} cm^2/s, ρ=1.3 g/cc, p_{O2}=63 cmHg, ß=1.

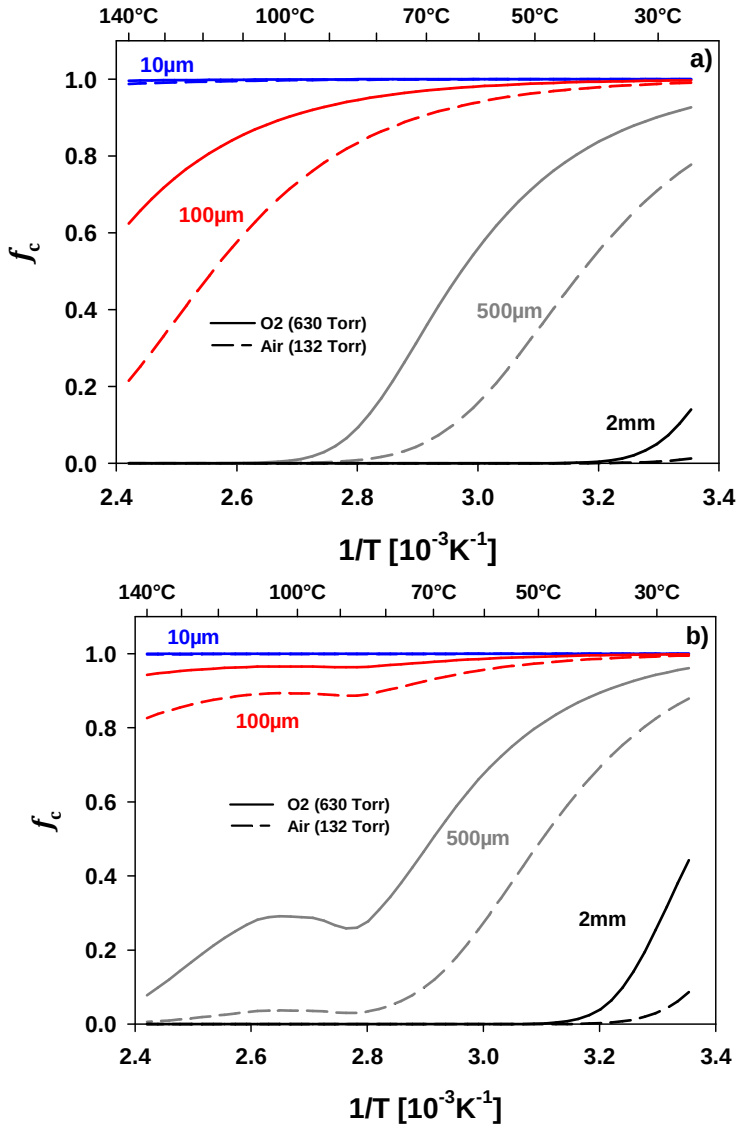

Fig. 8 Flux correction factors for epoxies as a function of temperature and film thickness. Curves were generated with interpolated permeability (see Fig.3) and oxidation rate values [37], and using β= 5 (normalized with ambient partial pressure). Permeative fluxes at elevated temperature are reduced due to significant material oxidation, even for a 100 µm film. a) Epon828/A2049; b) Epon828/D230 with the irregular behavior at ~ 90 °C due to T_g with changes in *S*.

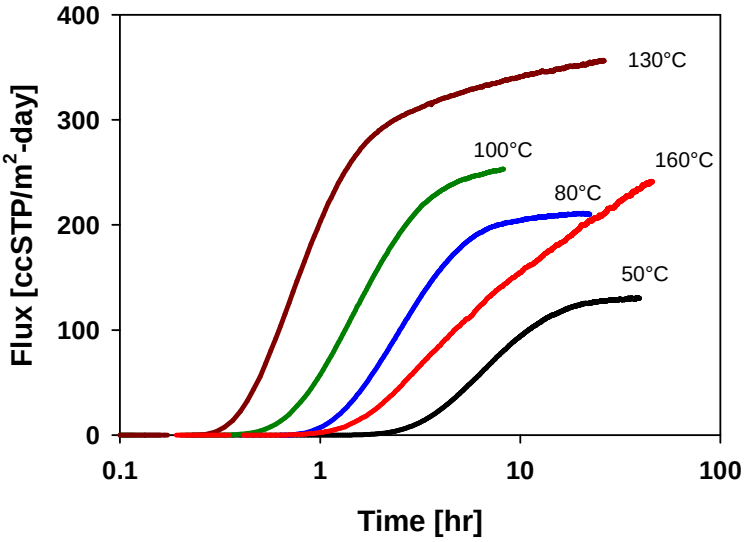

Fig. 9 Reduction of flux due to oxidation for a 505 µm MVK-14 material for pure O_2 (630 Torr). The flux at 160°C is lower than at 130°C and equilibrium times are extended.

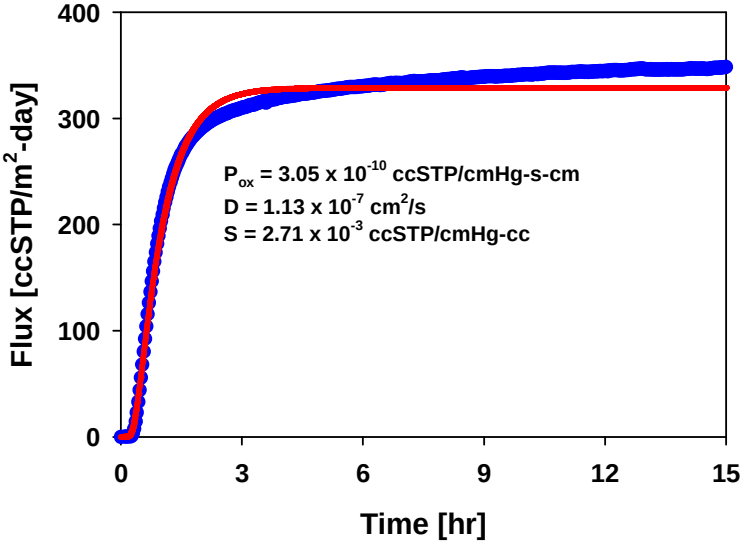

Fig. 10 Example of measured permeative flux and its fit for MVK-14 material for pure O_2 at 630 Torr and 130°C. There is some evidence for an evolving subtle drift in equilibrium (non-Fickian component) for extended times at elevated temperatures.

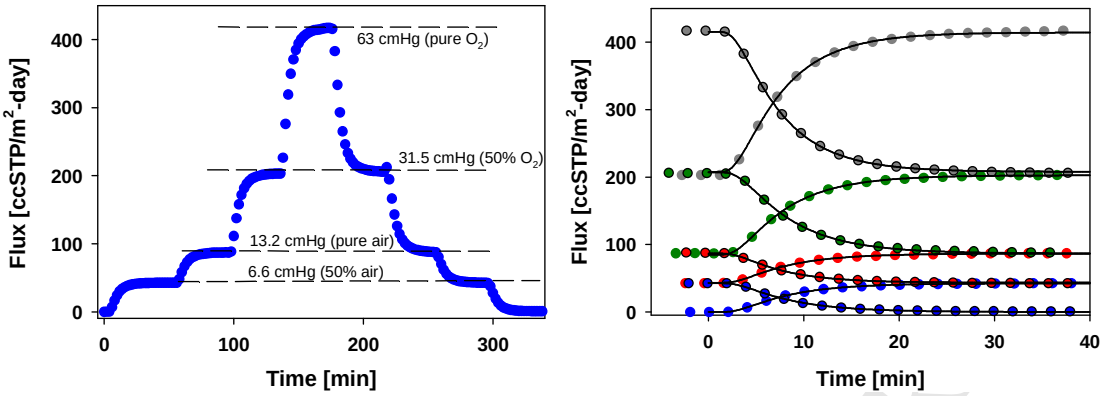

Fig. 11 Example of feed gas compositional changes for O_2 flux through Kapton film (50 µm) at 65°C for different O_2 partial pressures, i.e. compositional variation at 63 cmHg total pressure (O_2 + N_2). The enlarged individual gas switching experiments are shown on the right. These experiments yield consistent permeability (included in Fig. 13) and diffusivity.

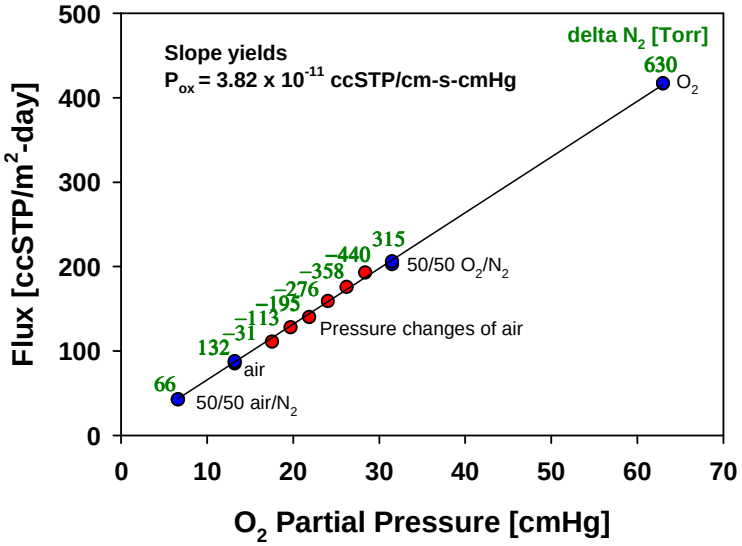

Fig.12 Flux for 50 µm Kapton film at 65°C as a function of absolute O_2 partial pressure, obtained by feed-gas compositional changes and pressure changes of air (ambient O_2 pressure in ABQ equals 13.2 cmHg). Counter (positive N_2 pressure differential with regard to sensor side flow) and parallel N_2 permeation (negative N_2 pressure differential) occurred during these measurements showing that O_2 permeation is completely independent of competing N_2 permeation processes. The absolute N_2 partial pressure difference as pick-up gas (fixed at 63 cmHg) minus feed-gas is noted on each data point. The resulting permeability data have been added to Fig. 13.

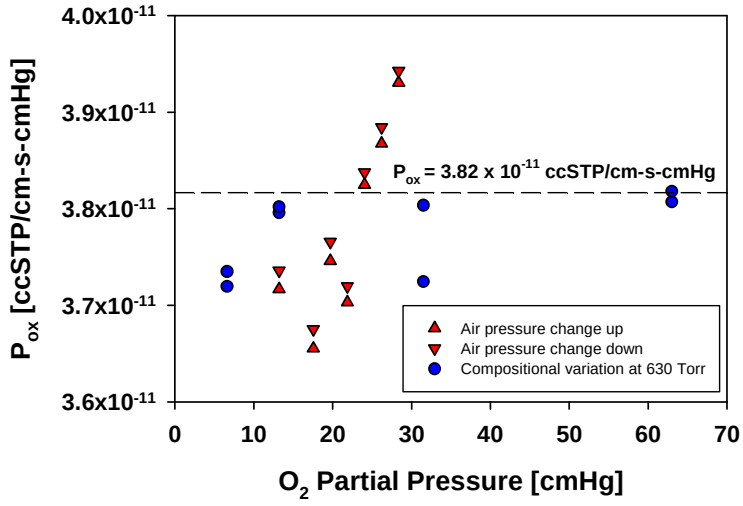

Fig.13 Permeability for a Kapton film (50 µm) at 65°C determined from multiple total pressure (air) and compositional variations at 630 Torr, showing only small variance.

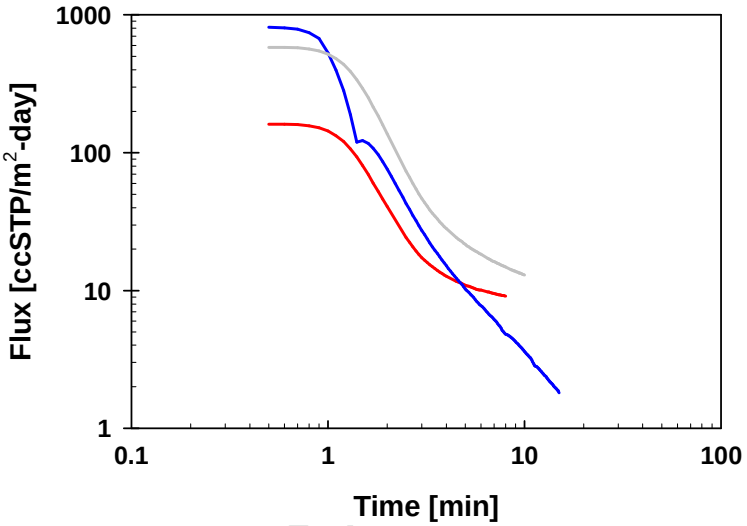

Fig.14 O_2 flux through Kapton polymer film followed by switch to pure N_2 carrier gas (at time zero) achieved by bypassing the external permeation cell. This results in an instantaneous change in the composition of the N_2 pick-up gas flow to the detector and a rapid but delayed decline in detector response. The highest signal decay was acquired over two sensitivity settings given by an automatic instrumental resistor switch (small dip in the blue curve).

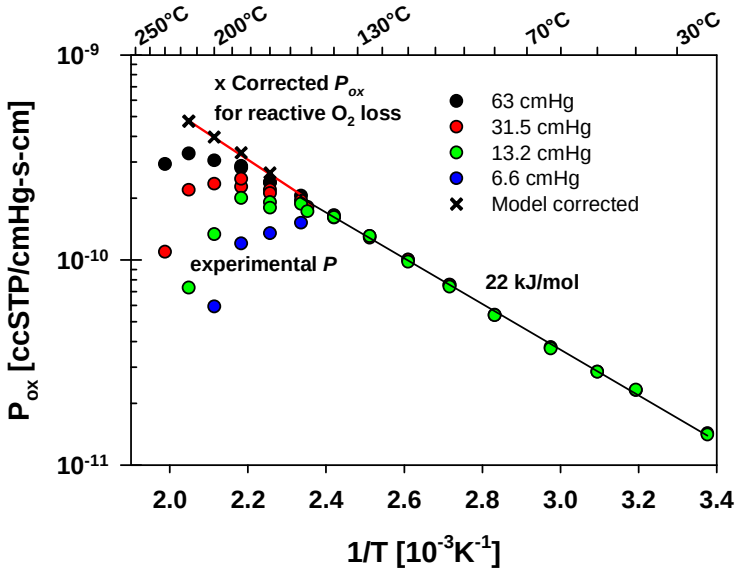

Fig. 15 Permeability for Kapton measured on 50 µm film showing the strong influence of DLO in the 160 to 220°C regime. The underlying material property can be determined using the reactive transport model, which enables corrections for oxidative loss.

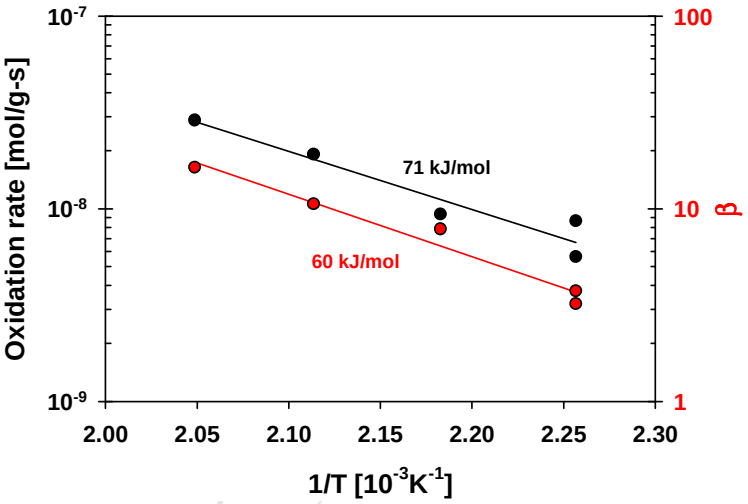

Fig. 16 The large data set of *P* taken for different partial pressures in Fig. 15 can be corrected for oxidation with the reactive transport model, which in parallel provides guidance on underlying oxidation rate and *β*.

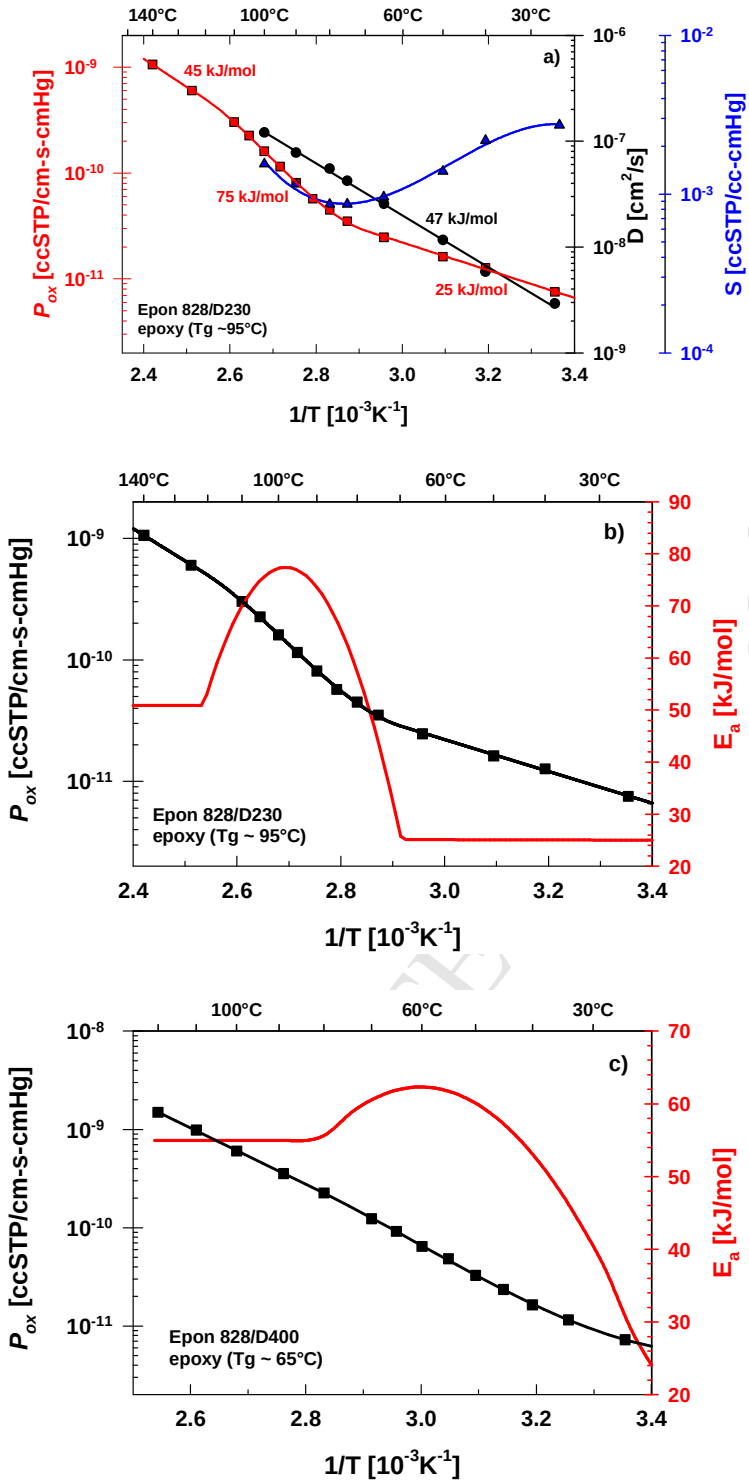

Fig.17 Overview of the effects of T_g on O_2 permeability. a) Plot for 828/D230 showing that a transition in solubility is the origin for the transition in P_{ox}. Permeability and its temperature dependent E_a (derivative in the Arrhenius plot) for 828/D230 (b) and 828/D400 (c).

Table 1: Summary of P_{ox}, D, S data obtained in this study. These data were taken at minimum as an average of 4 measurements for air and O_2 with up and down repeats for flux as shown in Fig. 1. Note: Data were not always taken at identical temperatures with some taken at plus (a) or minus 5°C (b) from the temperature denoted in the column (i.e. *P* for MVK-14 for '125°C' relates to 120°C and for '95°C' to an actual temperature of 100°C.)

Permeability [ccSTP/cm-s-cmHg]	25°C	40°C	50°C	65°C	80°C	95°C	110°C	125°C	140°C
828/A2049	1.40E-11	2.40E-11	3.30E-11	5.10E-11	7.70E-11	1.20E-10	1.60E-10	2.40E-10	3.10E-10
828/D230	7.53E-12	1.27E-11	1.62E-11	2.47E-11	4.49E-11	1.15E-10	3.03E-10	6.02E-10	1.06E-09
828/D400	7.26E-12	1.65E-11	3.28E-11	9.17E-11	2.26E-10		9.87E-10	1.49E-09[b]	
Kapton	1.43E-11	2.32E-11	2.85E-11	3.88E-11	5.39E-11	7.51E-11	9.94E-11	1.30E-10	1.63E-10
MVK-14	7.10E-11		1.16E-10		1.88E-10	2.60E-10[a]		3.03E-10[b]	4.28E-10
Polypropylene	1.97E-10	6.59E-10	9.38E-10	2.02E-09	3.44E-09	6.47E-09	1.23E-08	1.68E-08[b]	
Diffusivity [cm^2/s]									
828/A2049	4.97E-09	1.01E-08	1.67E-08	3.28E-08	5.22E-08	7.66E-08			
828/D230	2.92E-09	5.84E-09	1.17E-08	2.56E-08	5.48E-08	1.20E-07[a]			
828/D400	5.36E-09	1.69E-08	3.47E-08	8.88E-08	1.90E-07	2.87E-07[b]	5.37E-07		
Kapton	1.19E-09	2.79E-09	4.36E-09	7.23E-09	1.49E-08				
MVK-14	4.97E-09		1.46E-08		3.97E-08	6.86E-08[a]		1.12E-07[b]	1.97E-07
Polypropylene	2.12E-07	6.05E-07	9.70E-07	1.88E-06	3.29E-06	5.77E-06	1.29E-05	1.48E-05[a]	
Solubility [ccSTP/cc-cmHg]									
828/A2049	2.82E-03	2.28E-03	1.92E-03	1.55E-03	1.44E-03	1.57E-03			
828/D230	2.72E-03	2.18E-03	1.39E-03	9.59E-04	8.62E-04	1.55E-03[a]			
828/D400	1.36E-03	9.73E-04	9.45E-04	1.03E-03	1.19E-03	1.24E-03[b]	1.84E-03		
Kapton	1.20E-02	8.28E-03	6.54E-03	5.19E-03	3.61E-03				
MVK-14	1.43E-02		7.94E-03		4.74E-03	3.79E-03[a]		2.70E-03[b]	2.18E-03
Polypropylene	9.34E-04	1.09E-03	9.70E-04	1.08E-03	1.05E-03	1.12E-03	1.07E-03	1.46E-03[a]	

Oxygen diffusivity and permeation through polymers at elevated temperature

Mathew Celina and Adam Quintana

Graphical Table of Content (TOC)

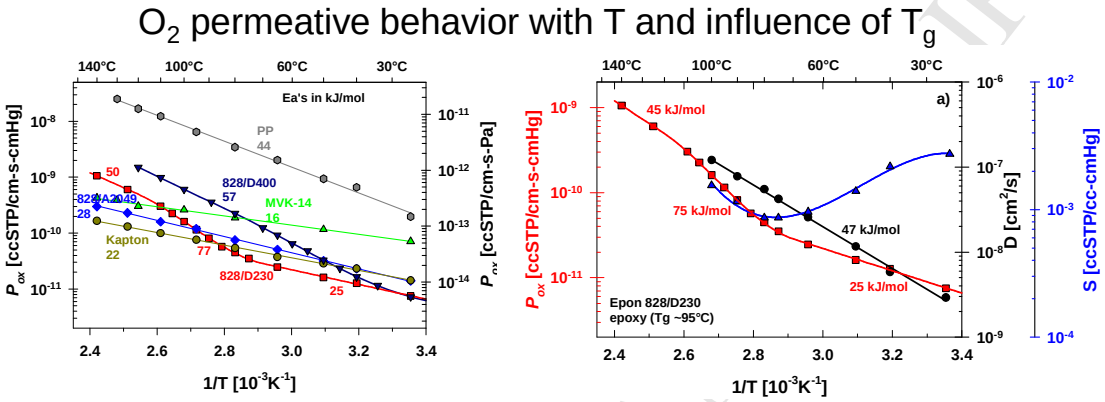

Highlights:

- O_2 permeation through polymers at elevated temperature competes with oxidation
- Mathematical model decouples physical diffusion from parallel chemical reactions
- *P*, *D*, *S* for O_2 quantified for different polymers with temperature
- Improved data for O_2 transport and material characterization
- Solubility but not diffusivity changes through glass transition

Permeability [ccSTP/cm-s-cmHg]	25°C	40°C	50°C	65°C	80°C	95°C	110°C	125°C	140°C
828/A2049	1.40E-11	2.40E-11	3.30E-11	5.10E-11	7.70E-11	1.20E-10	1.60E-10	2.40E-10	3.10E-10
828/D230	7.53E-12	1.27E-11	1.62E-11	2.47E-11	4.49E-11	1.15E-10	3.03E-10	6.02E-10	1.06E-09
828/D400	7.26E-12	1.65E-11	3.28E-11	9.17E-11	2.26E-10		9.87E-10	1.49E-09[b]	
Kapton	1.43E-11	2.32E-11	2.85E-11	3.88E-11	5.39E-11	7.51E-11	9.94E-11	1.30E-10	1.63E-10
MVK-14	7.10E-11		1.16E-10		1.88E-10	2.60E-10[a]		3.03E-10[b]	4.28E-10
Polypropylene	1.97E-10	6.59E-10	9.38E-10	2.02E-09	3.44E-09	6.47E-09	1.23E-08	1.68E-08[b]	
Diffusivity [cm^2/s]									
828/A2049	4.97E-09	1.01E-08	1.67E-08	3.28E-08	5.22E-08	7.66E-08			
828/D230	2.92E-09	5.84E-09	1.17E-08	2.56E-08	5.48E-08	1.20E-07[a]			
828/D400	5.36E-09	1.69E-08	3.47E-08	8.88E-08	1.90E-07	2.87E-07[b]	5.37E-07		
Kapton	1.19E-09	2.79E-09	4.36E-09	7.23E-09	1.49E-08				
MVK-14	4.97E-09		1.46E-08		3.97E-08	6.86E-08[a]		1.12E-07[b]	1.97E-07
Polypropylene	2.12E-07	6.05E-07	9.70E-07	1.88E-06	3.29E-06	5.77E-06	1.29E-05	1.48E-05[a]	
Solubility [ccSTP/cc-cmHg]									
828/A2049	2.82E-03	2.28E-03	1.92E-03	1.55E-03	1.44E-03	1.57E-03			
828/D230	2.72E-03	2.18E-03	1.39E-03	9.59E-04	8.62E-04	1.55E-03[a]			
828/D400	1.36E-03	9.73E-04	9.45E-04	1.03E-03	1.19E-03	1.24E-03[b]	1.84E-03		
Kapton	1.20E-02	8.28E-03	6.54E-03	5.19E-03	3.61E-03				
MVK-14	1.43E-02		7.94E-03		4.74E-03	3.79E-03[a]		2.70E-03[b]	2.18E-03
Polypropylene	9.34E-04	1.09E-03	9.70E-04	1.08E-03	1.05E-03	1.12E-03	1.07E-03	1.46E-03[a]	